JACS Au
AN OPEN ACCESS JOURNAL OF THE AMERICAN CHEMICAL SOCIETY

pubs.acs.org/jacsau
Article

Atomic-Level Dissection of DC-SIGN Recognition of *Bacteroides vulgatus* LPS Epitopes

Ferran Nieto-Fabregat, Qian Zhu, Corinne Vivès, Yunqin Zhang, Angela Marseglia, Fabrizio Chiodo, Michel Thépaut, Diksha Rai, Suvarn S. Kulkarni, Flaviana Di Lorenzo, Antonio Molinaro, Roberta Marchetti, Franck Fieschi, Guozhi Xiao, Biao Yu,* and Alba Silipo*

Cite This: *JACS Au* 2024, 4, 697–712

Read Online

ACCESS | Metrics & More | Article Recommendations | Supporting Information

ABSTRACT: The evaluation of *Bacteroides vulgatus* mpk (BVMPK) lipopolysaccharide (LPS) recognition by DC-SIGN, a key lectin in mediating immune homeostasis, has been here performed. A fine chemical dissection of BVMPK LPS components, attained by synthetic chemistry combined to spectroscopic, biophysical, and computational techniques, allowed to finely map the LPS epitopes recognized by DC-SIGN. Our findings reveal BVMPK's role in immune modulation via DC-SIGN, targeting both the LPS O-antigen and the core oligosaccharide. Furthermore, when framed within medical chemistry or drug design, our results could lead to the development of tailored molecules to benefit the hosts dealing with inflammatory diseases.

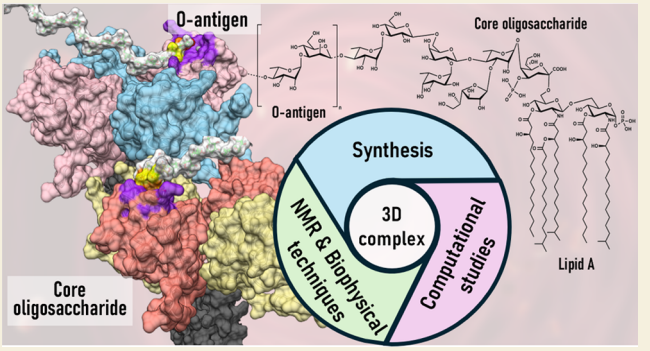

KEYWORDS: *Bacteroides vulgatus lipopolysaccharide, DC-SIGN, lectins, gut microbiota, NMR spectroscopy*

INTRODUCTION

The human gastrointestinal tract harbors the highest population of microorganisms, the gut microbiota (GM), a complex and dynamic combination of commensal bacteria, fungi, and viruses, crucial for the activation, development, and functional maturation of mucosal and systemic immune systems.[1] GM is therefore proposed to shape host immunity and maintain homeostasis, provide benefits by detoxification and nutrient processing from the dietary income, and protect against external pathogens by enhancing the intestinal barrier through direct (as competition for common nutrients and niches) and indirect (as enhancement of host defense) mechanisms.[2−4]

The immune system is well-equipped with a wide range of innate pattern-recognition receptors (PRRs) that sense specific microbial constituents named MAMPs (microbe-associated molecular patterns). Known for being the major component of the external leaflet of Gram-negative outer membrane, LPS (lipopolysaccharide) is a renowned MAMP crucial in the host−microbe dialogue as it can mediate either beneficial or detrimental interactions, such as colonization, virulence, adhesion, symbiosis, and tolerance.[5] LPSs are elicitors of host immune responses in a structure-dependent manner, and even slight structural changes may strongly affect and tune their function and role and modulate host immune recognition and receptor targeting.[5,6] Structurally and biosynthetically, LPS is a heat-stable amphiphilic molecule constituted by three different motifs: the lipid A, the core oligosaccharide, and the O-antigen polysaccharide (OPS).[7]

Among the four different PRR families, lectin receptors represent a broad group of nonimmunoglobulin proteins recognizing glycan epitopes exposed on the cell surface[8] without displaying any enzymatic activity though being involved in antimicrobial immunity. Indeed, lectins occur ubiquitously in nature and play a key role in cell−cell/cell−pathogen communications, immune cell function regulation, and cellular trafficking *inter alia*.[9] They include both transmembrane and soluble extracellular proteins and are increasingly emerging as immune receptors of bacterial LPS and envelope glycoconjugates.[10,11] C-type lectin (CTL) represents the biggest and most extended lectin class (soluble or membrane-bound), able to recognize cell surface glycans on self-proteins as well as on viruses, bacteria, and parasites. Soluble CTLs, expressed mostly by myeloid antigen-presenting cells such as macrophages and dendritic cells, can function as opsonins that facilitate phagocytic uptake, activation of the complement pathway, modulation of inflammation, and

Received: November 28, 2023
Revised: January 24, 2024
Accepted: January 25, 2024
Published: February 12, 2024

https://doi.org/10.1021/jacsau.3c00748
JACS Au 2024, 4, 697−712

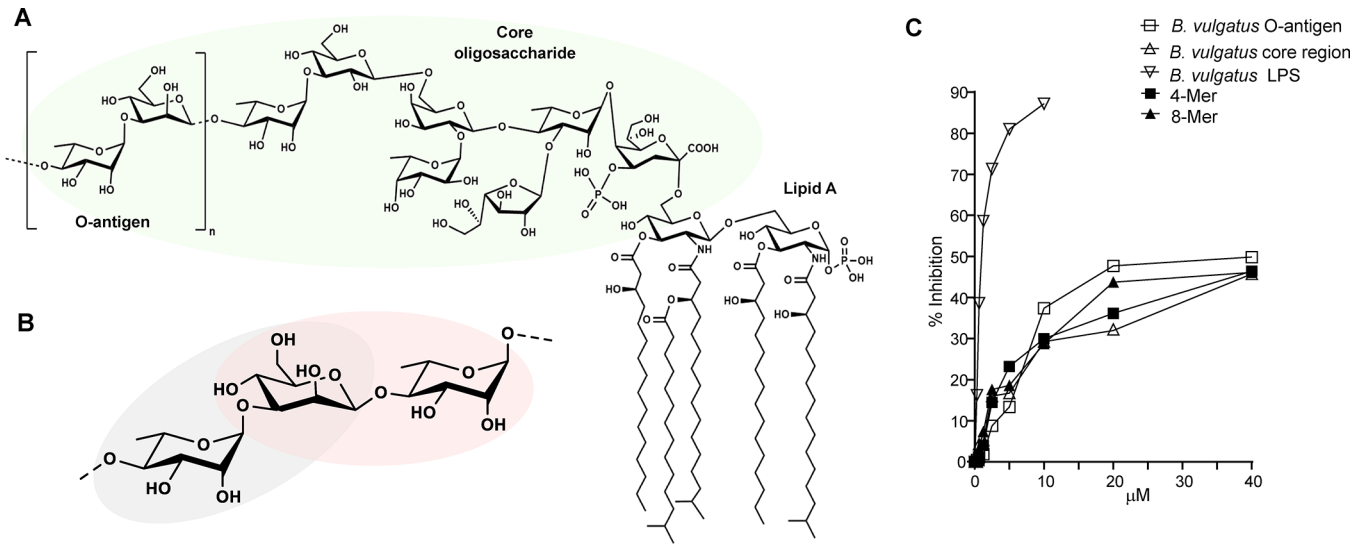

Figure 1. *Bacteroides vulgatus* mpk structure. (A) BVMPK complete LPS structure. (B) O-antigen disaccharide repeating unit constituted by an α-L-rhamnopyranose and a β-D-mannopyranose. Circled in green and gray/pink are the core and O-antigen LPS portions here evaluated in their interaction with DC-SIGN. (C) ELISA analysis of the competition binding of *B. vulgatus* core and O-antigen and LPS to human C-type lectin DC-SIGN. The competition experiments have been performed three times showing similar results; the graph shows data of one of these experiments. The two synthetic oligomers, 4-Mer and 8-Mer, were also added to the plate for comparison.[24]

Scheme 1. Synthesis of the Rhamnose-Terminated 3-Mer 4 and 5-Mer 7[a]

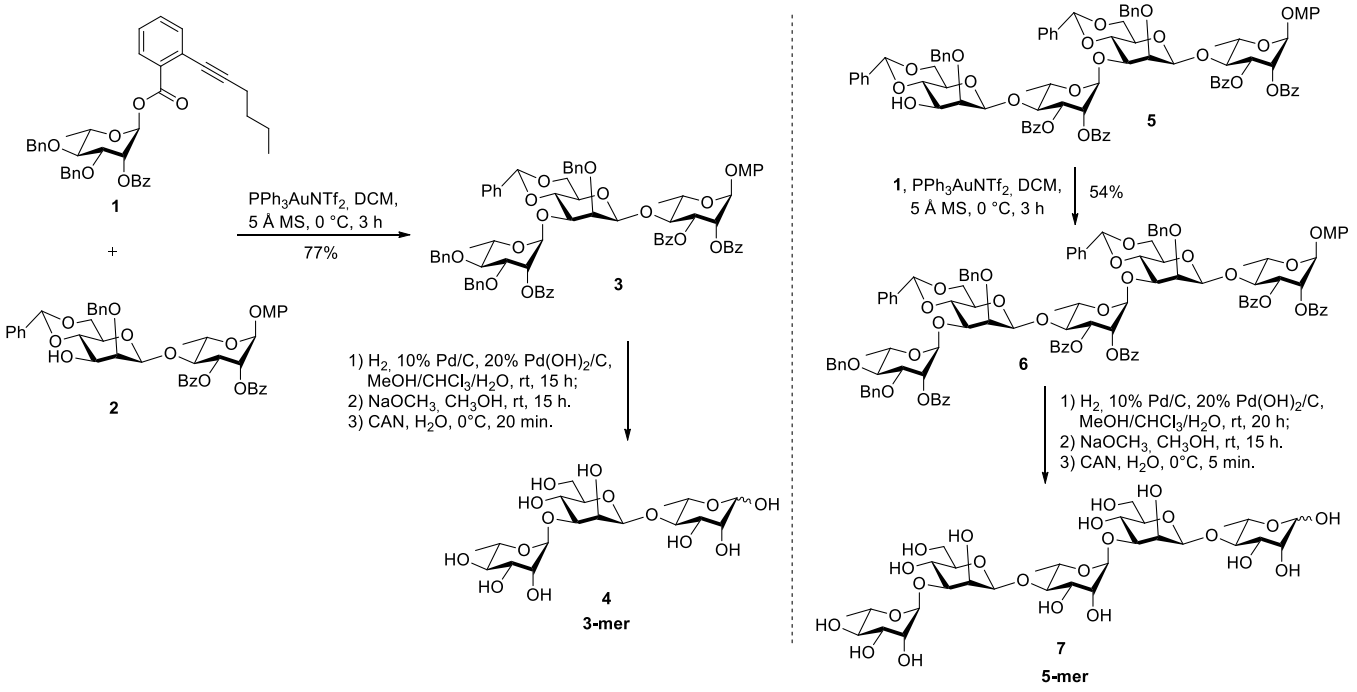

[a]Bn, benzyl; Bz, benzoyl; CAN, cerium(IV) diammonium nitrate; MP, 4-methoxylphenyl; PPh_3AuNTf_2, gold(I) bis(trifluoromethanesulfonyl)-imidate; MS, molecular sieve.

inhibition or direct killing of a wide variety of microorganisms. Their carbohydrate recognition domain (CRD) is key to delineating the glycan epitope recognized and accommodated in the binding site[12]; in most cases, the interaction takes place in a Ca^{2+}-dependent manner, with DC-SIGN (dendritic cell-specific intracellular adhesion molecules (ICAM)-3 grabbing nonintegrin), also known as CD209, being a perfect example.[13−15] The DC-SIGN family includes type II transmembrane glycoprotein receptors composed of a neck region followed by the CRD, having the N-terminus in the cytosol and the C-terminus exposed outside the lipid bilayer. Structurally, the most interesting portion of CRD is the loop that extends outside the surface of the protein, which is involved in the formation of two cavities that can accommodate the Ca^{2+} ions, key for the carbohydrate binding properties of DC-SIGN. In particular, the principal binding site, constituted by the EPN motif (Glu347, Pro348, and Asn349) together with Glu354 and Asn365 residues, drives carbohydrate coordination and delineates the specificity for the recognized ligands.[16−18]

https://doi.org/10.1021/jacsau.3c00748
JACS Au 2024, 4, 697−712

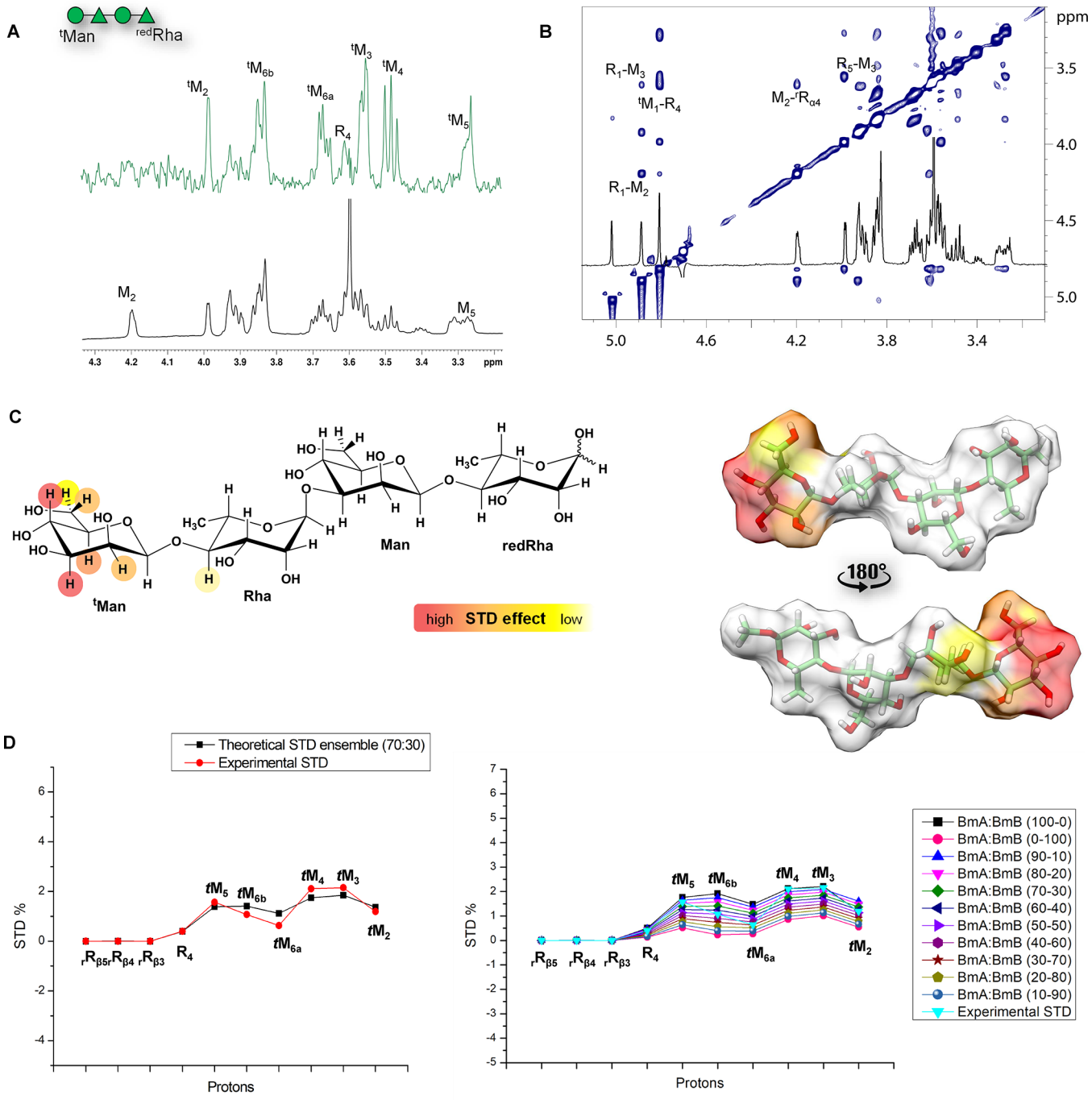

Figure 2. NMR interaction studies between 4-Mer and DC-SIGN. (A) 4-Mer ligand schematic structure sketched according to SNFG nomenclature. STD NMR zoomed spectrum (full spectrum Figure S2A). ^{1}H NMR reference spectrum (bottom) and 1D STD NMR spectrum (up) of the 1:30 mixture of DC-SIGN:4-Mer. (B) tr-NOESY NMR on the 1:20 mixture of DC-SIGN:4-Mer. (C) 2D and 3D representation of the interacting epitope map of the interaction between 4-Mer and DC-SIGN derived from STD NMR data and computational studies. (D) CORCEMA-ST analysis was derived from the most representative poses of the DC-SIGN/4-Mer complex. The analysis of the contribution of binding mode A (**BmA**) and binding mode B (**BmB**) to the ensemble was performed by analyzing the quality of the prediction by the NOE R-factor (see Table S2), determining that the contribution to the ensemble was 70% for **BmA** and 30% for **BmB**, similar results as those obtained from the analysis of the MD simulation, the most demonstrating the best fit between the ensemble theoretical (blue) and experimental (red) STD data.

The *Bacteroides* genus includes obligate anaerobic Gram-negative bacteria, ubiquitous commensals, and important beneficial members of the human colon.[19,20] An example is *Bacteroides vulgatus* whose oral administration can repair the colonic gap junction and prevent colitis in a strain-dependent manner[21]; likewise, *B. vulgatus* mpk (BVMPK)[5,22] plays a significant role in protecting against *Escherichia coli*-induced colitis or *Yersinia enterocolitica*-induced inflammation, reducing intestinal inflammation and repairing the tissue damage.[5,20] BVMPK LPS has been established as a weak agonistic LPS, as it does not promote a pro-inflammatory response in both human *in vitro* and murine *in vivo* experiments.[23]

https://doi.org/10.1021/jacsau.3c00748
JACS Au 2024, 4, 697−712

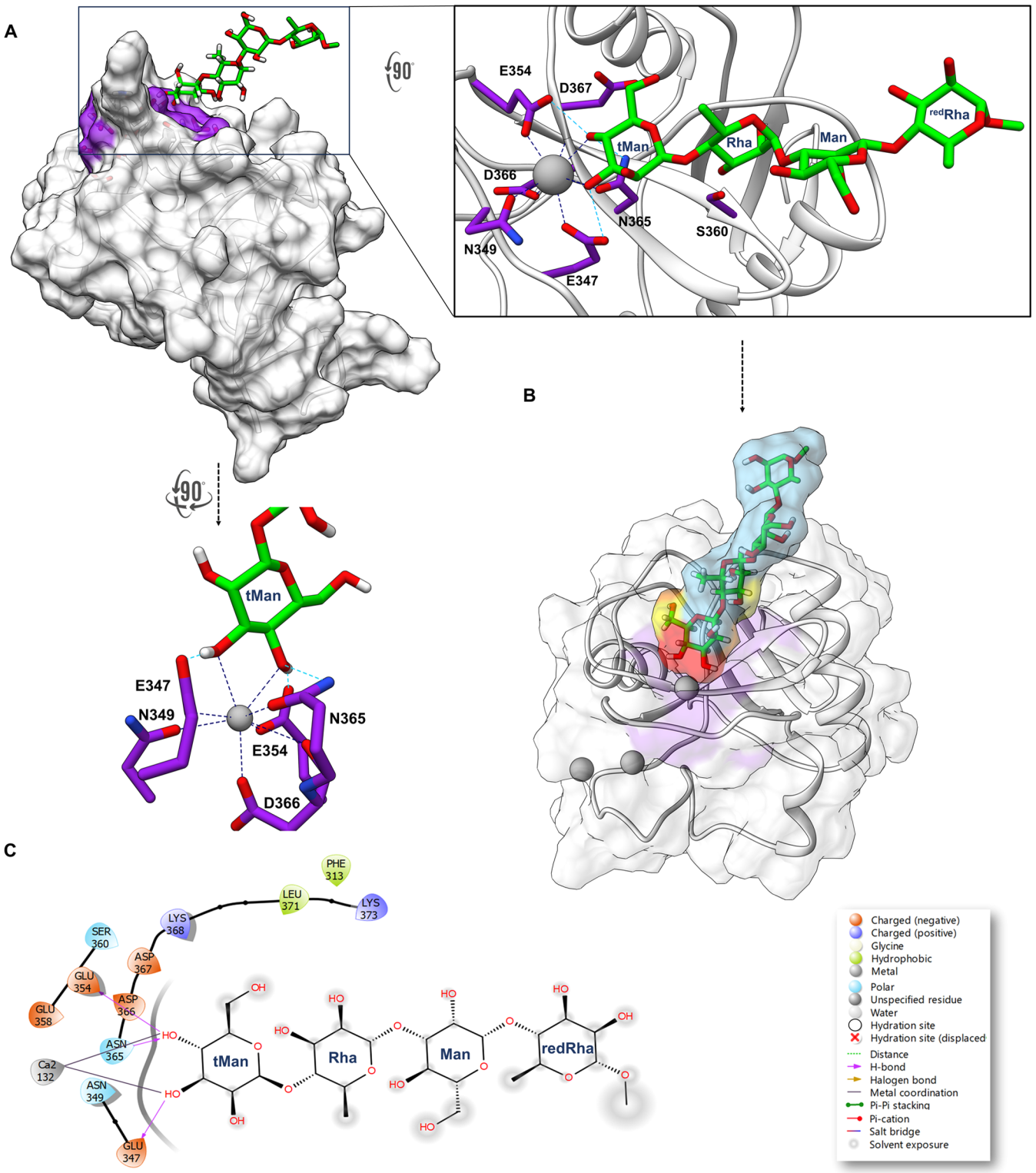

Figure 3. MD simulation analysis of the *major binding mode A* for the DC-SIGN:4-Mer complex **A**) 3D model of DC-SIGN − 4-Mer complex with the protein amino acids involved in the interaction highlighted in purple. Close-up view of a representative pose from the most populated MD family (top right) and the tMan bound to the principal Ca^{2+}. The main amino acids involved in the binding are colored in purple and the Ca^{2+} ion in gray. The ligand is colored according to SNFG. Ca^{2+} coordination bonds are shown as dashed blue lines while the observed H-bond interactions are indicated by dashed cyan lines. **B**) 3D representation of the interaction with the ligand surface colored according to the STD NMR results. **C**) **BmA** two-dimensional plot representing the interactions between 4-Mer and DC-SIGN binding pocket residues.

A major role of DC-SIGN in mediating host immune recognition of bacterial envelope glycans has been proposed,[11,16−18,24] including its involvement in TLR/immune cell activation. Our working hypothesis came from the evidence that BVMPK LPS not only exerts a protective role for the host by stimulating the release of anti-inflammatory

https://doi.org/10.1021/jacsau.3c00748
JACS Au 2024, 4, 697−712

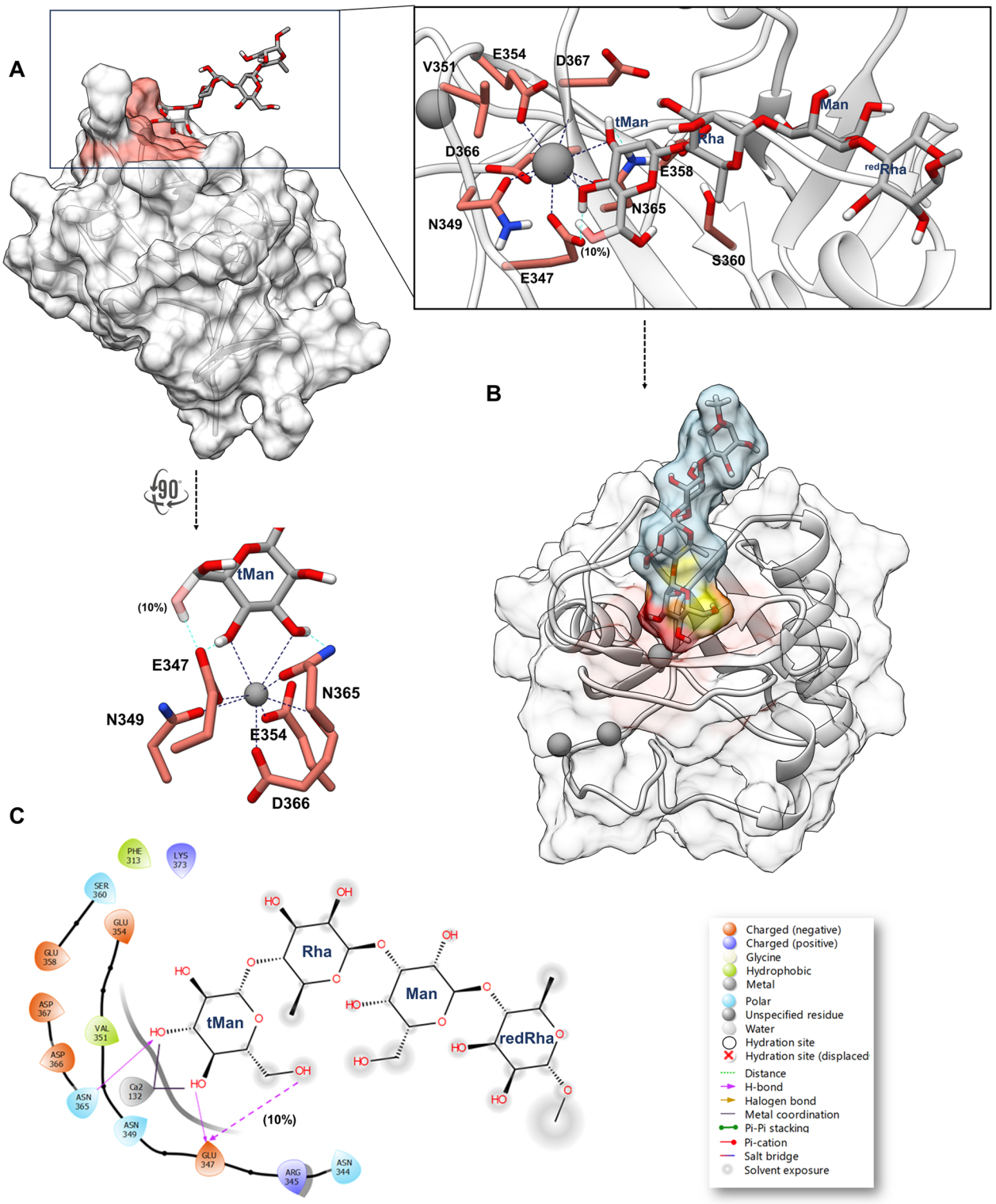

Figure 4. MD simulation analysis of the *minor binding mode B*, interaction between 4-Mer and DC-SIGN. (A) 3D model of the DC-SIGN−4-Mer complex with the protein amino acids involved in the interaction highlighted in salmon. Close-up view of a representative pose from the most populated MD family (top right) and the tMan bound to the principal Ca^{2+}. The main amino acids involved in the binding are colored in purple and the Ca^{2+} ion in gray. The ligand is colored according to SNFG. Ca^{2+} coordination bonds are shown as dashed blue lines, while the observed H-bond interactions are indicated by dashed cyan lines. (B) 3D representation of the interaction with the ligand surface colored according to the STD NMR results. (C) **BmB** two-dimensional plot representing the interactions between 4-Mer and DC-SIGN binding pocket residues.

cytokines[23] but also displays a selective affinity for human lectin DC-SIGN,[24] which is associated with gut lymphoid tissue and homeostasis. Therefore, we here sought to dissect BVMPK LPS recognition and interaction with DC-SIGN, and due to the uniqueness of the LPS structure and the relevance of glycan motifs in modulating the immune functions, we focused on the molecular evaluation of *B. vulgatus* mpk LPS components in their interaction with DC-SIGN, by means of

https://doi.org/10.1021/jacsau.3c00748
JACS Au 2024, 4, 697−712

synthetic, spectroscopic, and biophysical methods. In particular, we used synthetic LPS glycoforms containing either BVMPK O-antigen variable repeating units or the core region (Figure 1 and Scheme 1), to evaluate their contribution to the binding. By this combination of complementary approaches, we demonstrated that DC-SIGN effectively recognizes and binds different constituents of BVMPK LPS, located either in the core or in the O-antigen portion, therefore highly diminishing the possibility of a nonspecific interaction. This novel type of recognition demonstrates the importance of *B. vulgatus* LPS glycans' complexity and variability in mediating host immune recognition by DC-SIGN.

RESULTS

DC-SIGN Recognition of BVMPK LPS

Inspired by the already probed interaction between synthetic O-antigen oligomers and DC-SIGN,[24] we further investigated DC-SIGN binding to *B. vulgatus* LPS constituents (Figure 1), particularly the isolated core oligosaccharide (Figure 1), by competition ELISA experiments (Figure 1). To better compare the results, also two representative synthetic oligomers, namely, the 4-Mer and 8-Mer (Figure 1 and Figure S1), were added to the plate. Notably, in all cases, ELISA assays detected binding, since either LPS component (the O-antigen, as expected, and more importantly the core portion) showed the ability to inhibit LPS binding to DC-SIGN in a typical dose−response curve (Figure 1C and Figure S1). Given the above, BVMPK LPS recognition by the recombinant extracellular domain of DC-SIGN was evaluated using a combination of synthetic approaches, NMR spectroscopy, and computational and biophysical techniques as follows.

BVMPK LPS O-Antigen−DC-SIGN Interaction

BVMPK OPS consists of [→ 3)-β-D-Man-(1 → 4)-α-L-Rha-(1 →] disaccharide repeating units (RU); therefore, oligomers of different lengths, terminating either with Rha or with Man, were *ad hoc* synthesized (Figure 1 and Figure S1), those terminating with Man as already described (Figure S1A),[24] and those terminating with Rha (Figure 1 and Figure S1) by the synthetic approach shown in Scheme 1 and in the Supporting Information). These oligomers with variable numbers of RU contained an L-rhamnose residue (^{red}Rha) at the reducing portion, while the nonreducing end was capped alternatively by a terminal mannose or a terminal rhamnose residue (tMan; 2-Mer, 4-Mer, and 8-Mer; Figure S1A; tRha, 3-Mer, and 5-Mer; Figure S1B). They were thoroughly evaluated in their interaction with DC-SIGN, with the aim of disclosing the role, if any, played by the length of the saccharide chain.

O-Antigen Oligomers with tMan-Binding Studies

Binding studies were conducted on the different *B. vulgatus* oligomers with comparable results. STD NMR experiments[25] were used to unveil the binding epitopes and showed that the contact between DC-SIGN and the oligos took place mostly at the terminal portion. In particular, the STD analysis of the mixture DC-SIGN: 4-Mer (Figure 2 and Figure S2) allowed depiction of a binding epitope where the main interaction occurred through the tMan residue, which showed the highest STD enhancements. Thus, the interacting epitope included H3 and H4 of tMan, which showed the strongest STD effects, followed by a good contribution of H5 and finally slighter involvement of the remaining ring protons. Instead, the L-Rha directly linked to the terminal Man showed a low STD response with H4, further confirming that tMan was the main moiety in contact with DC-SIGN. Conversely, no STD effects were observed for either the inner Man or the ^{red}Rha unit, indicative of being solvent exposed. NMR binding studies with longer ligands, such as 8-Mer showed comparable NMR derived binding epitope (Figure S3).

The bioactive conformation adopted by the ligand upon binding was explored by tr-NOESY experiments (Figure 2B, spectra on 4Mer). A comparison of spectra acquired in the free[24] and bound states unveiled no significant changes, confirming an extended conformation of the glycan chain, therefore unchanged once complexed with DC-SIGN (see Discussion below, Figure 2C, and Table S1). Further details on the molecular recognition features were disclosed, complementing NMR-derived binding data to computational studies as follows. Once the energetically accessible conformational regions of glycosidic torsion angles (α-L-Rha-(1 → 3)-β-D-Man and β-D-Man-(1 → 4)-α-L-Rha) constituting BVMPK LPS O-antigen were obtained (Figure S4), a starting complex of the ligands with DC-SIGN was obtained by manual docking of the oligomers in the DC-SIGN monomeric subunit (from PDB 1SL4).[26] Thus, the terminal Man guided the superimposition of the oligomers in the binding site, taking as a reference the GlcNAc2Man3 unit present in 1SL4 pdb. The complex generation and its further optimization were performed using the Maestro suite of programs.[27] In detail, mannose can adopt two different orientations in the binding pocket as represented in Figure S5,[26,28,29] a binding mode with the 6-OH pointing toward the adjacent shallow groove (Figure 3 and Figure S5A, binding mode A, **BmA**), and, after rotating the ligand through the mannose residue by 180°, a second binding mode obtained with the axial 2-OH pointing toward the shallow groove (Figure 4 and Figure S5D, binding mode B, **BmB**).

Both accommodations, **BmA** and **BmB,** underwent extensive MD simulations, and the outcomes were subsequently evaluated on the basis of the NMR results to validate the findings. ϕ and ψ glycosidic torsion angles were sampled along the MD simulations in both free[24] and bound states to further evaluate the conformational behavior of BVMPK LPS O-antigen oligomers when complexed with DC-SIGN. Ensemble average interproton distances were extracted and translated into NOE contacts according to a full-matrix relaxation approach. The average distances obtained for the MD simulation from $\langle r^{-6} \rangle$ values were compared to those collected experimentally, and notably an excellent accordance between the experimental and calculated data was found (Table S1). Therefore, no significant differences in the ligands' extended conformation in both free and bound states were indeed found upon binding (see data on 4-Mer, Figure S4 and Figure 2). The most representative poses for the two binding modes **BmA** and **BmB** on the DC-SIGN/4mer complex were selected based on cluster analysis of the MD simulations and analyzed by means of the CORCEMA-ST program,[30] which allows to calculate predicted STD intensities for the proposed molecular models of ligand−receptor complexes. Therefore, CORCEMA-ST is a useful tool to validate the proposed 3D models and, as shown below, also to evaluate their relative abundance. Indeed, the results confirmed that in both **BmA** and **BmB** complexes, the terminal mannose was the main actor of the interaction, with a high contribution from H3 and H4 and an evident involvement of the other ring protons (Figure 2D). Indeed, in both cases, the highest STD value was predicted for tMan H3, in agreement with the experimental results. Conversely, no

https://doi.org/10.1021/jacsau.3c00748
JACS Au 2024, 4, 697−712

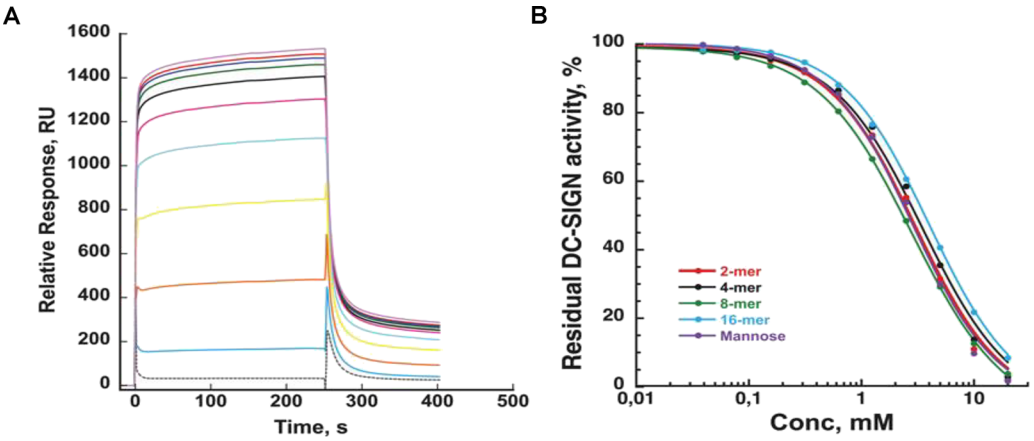

Figure 5. Inhibition of DC-SIGN interaction over BSA-Man surfaces with different oligomers of the O-antigen repeating unit. (A) Representative sensorgrams of the interaction and its inhibition with 2-Mer with increasing concentrations, by a multiplication factor of 2, starting from 40 μM up to 20 mM. (B) Inhibition curve obtained for 2-Mer, 4-Mer, 8-Mer, and 16-Mer.

saturation was predicted for the other sugar units except for the internal Rha, which participated in the binding with a good involvement only of the proton at position 4. In addition, according to the STD NMR results, no contribution was predicted for Man and ^{red}Rha residues. Nevertheless, overall, the calculated STD values for each individual binding mode did not completely align with the experimental STD NMR results, confirming the coexistence of two binding modes.

Thus, a theoretical bimodal binding equilibrium, involving a combination of **BmA** and **BmB**, was considered and the contribution of each binding mode to the interaction was determined as published.[31] Briefly, assuming that the signals of the STD spectra would be the weighted average of the accumulated saturations corresponding to the two binding modes, we could identify the ensemble of ligand-bound modes that best fit the experimental data assessing the quality of the CORCEMA-ST prediction by the R-NOE factor, a parameter that indicates the quality of the fit. We found that a satisfactory agreement between theoretical and experimental results was indeed achieved considering the following equilibrium of the two bound conformations in solution: **BmA** as *major binding mode* with a contribution around 70% and **BmB** as *minor binding mode* with a 30% contribution (NOE R-factor = 0.2; Table S2 and Figure 2D).

Representative poses of the less energetic and most populated clusters of the 4-Mer in the two binding modes **BmA** and **BmB** in Figures 3 and 4 show how the tMan residue was involved in the coordination with Ca^{2+} through hydroxyl moieties at positions 3 and 4 in the canonical binding mode.[28,32] Interestingly, RMSD calculations performed on protein backbone and ligand residues, with the first frame as reference, were indicative of the stability of the complexes, with comparable accommodation of the oligomers in the binding pocket (Figures 3 and 4 and Figure S5). Indeed, during the whole MD simulations, the tMan unit maintained the canonical coordination with the Ca^{2+} ion through positions 3 and 4, with the rest of the ligand solvent exposed. The occurring molecular interactions in the complexes were monitored and compared to the NMR-derived experimental data as follows (data on the 4-Mer in **BmA** and **BmB** are here discussed, and results on the other oligomers were comparable; see Figure S6). The Ca^{2+} ion located in the main DC-SIGN binding site and accommodated by Glu347, Pro348, and Asn349 plays a key role in the carbohydrate recognition and binding process, coordinating the tMan through the oxygen atoms of 3OH and 4OH. Notably, slight differences were observed between **BmA** and **BmB** binding modes. Specifically, in **BmA**, 3OH tMan acted as a hydrogen donor in the interaction with the Glu347 carboxylic moiety whereas tMan 4OH acted as a hydrogen donor in the interaction with the Glu354 carboxylic moiety and as an acceptor for Asn365 (Figure 3 and Figure S5B,C). However, in the case of **BmB**, due to the 180° rotation, a significant shift in the binding interactions occurred (Figure S7); tMan 3OH now functioned as a hydrogen acceptor, forming an interaction with Asn365, while tMan 4OH acted as a hydrogen donor, engaging with Glu347. In contrast to **BmA**, in **BmB**, Glu347 could also be observed forming a hydrogen bond with tMan 6OH during approximately 10% of the simulation time (Figure 4 and Figure S5E,F); this observation in **BmB** is in agreement with the STD NMR results and provides further explanation for the good contribution of H6 tMan to the interaction. The internal Rha unit along the MD simulation (Figures 3 and 4 and Figure S5) did not establish stable interactions, in particular hydrogen bonds with DC-SIGN; this fitted with the experimentally observed low STD contribution to the binding for the ring protons of internal Rha but H4, in full agreement with the predicted contribution by CORCEMA-ST calculations (Figure 2D).

The crucial role of Ca^{2+} in mediating the binding was further proved by NMR, as upon addition of perdeuterated EDTA to the sample, we observed a complete fading of STD NMR signals, evidence that no interaction occurred in the absence of calcium (Figure S8). Finally, we can propose a 3D complex of BVMPK O-antigen accommodated in the DC-SIGN binding site, where the tMan unit was essential for its recognition and binding in both **BmA** and **BmB** (Figures 3 and 4 and Figure S6).

O-Antigen Oligomers with tRha Synthesis and Binding Studies

Oligomers that terminate with L-Rha (Figure S1B) were synthesized as described below (Scheme 1 and the supporting text). Rhamnosyl *ortho*-hexynylbenzoate **1** was used as the glycosyl donor for α-rhamnosylation, which was activated by PPh_3AuNTf_2[33] at 0 °C and reacted with the disaccharide acceptor **2** and tetrasaccharide acceptor **5** to give 3-Mer **3** and

https://doi.org/10.1021/jacsau.3c00748
JACS Au 2024, 4, 697−712

Table 1. IC_{50} of Mannose and Different Oligomers of *B. vulgatus* OPS toward the DC-SIGN/BSA-Man Interaction Using an SPR Competition Assay

	Man	2-Mer	4-Mer	8-Mer	16-Mer
IC_{50} DC-SIGN (mM)	3.08 ± 0.03	3.31 ± 0.07	3.85 ± 0.09	3.08 ± 0.28	4.20 ± 0.17

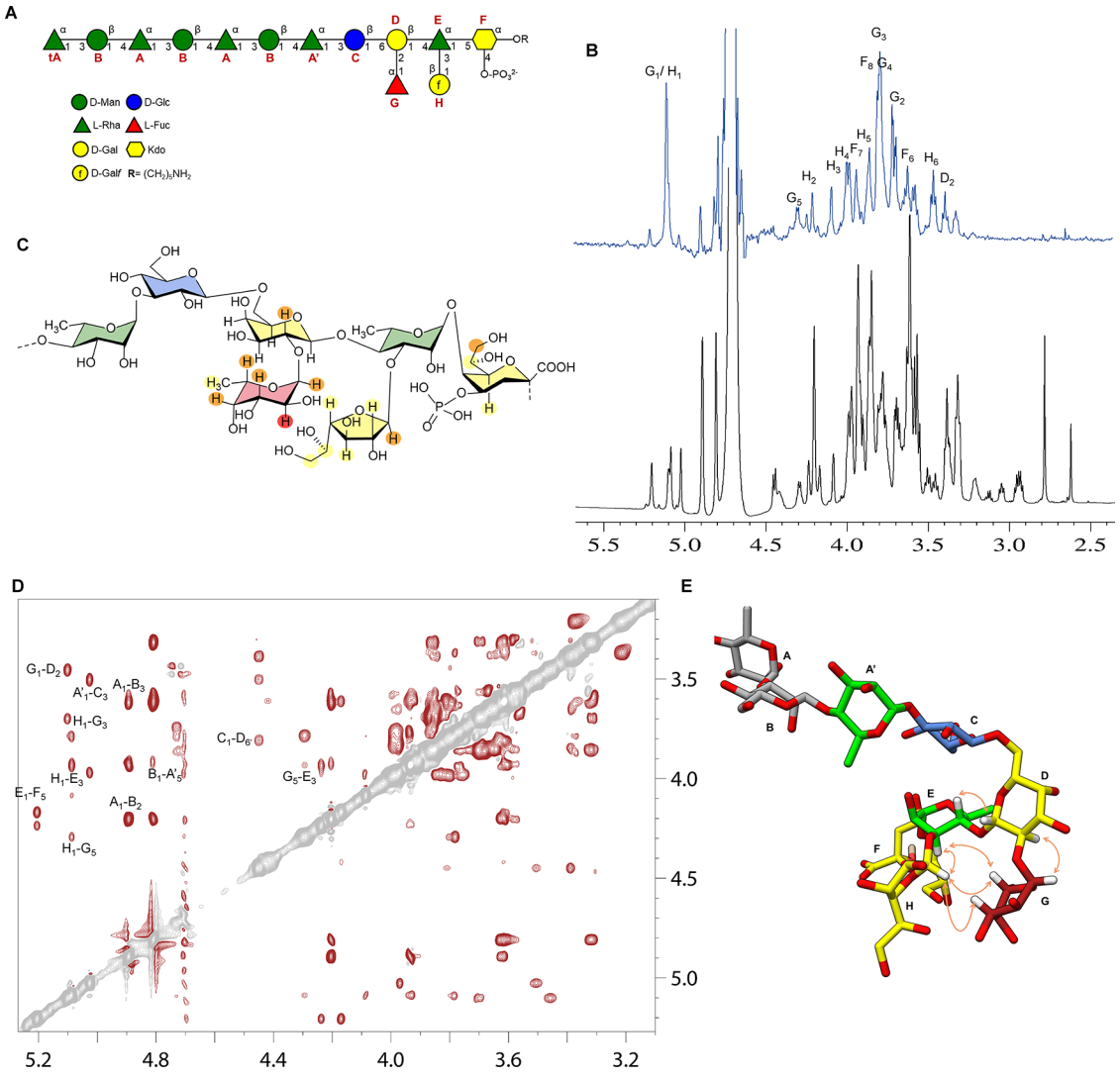

Figure 6. NMR interaction studies between tRha-LPS and DC-SIGN. (A) tRha-LPS tridecasaccharide schematic structure sketched according to SNFG nomenclature. (B) STD NMR zoomed spectrum (full spectrum Figure S23A). (Bottom) ^{1}H NMR reference spectrum and (top) 1D STD NMR spectrum of the 1:30 mixture of DC-SIGN: tRha-LPS. (C) 2D representation of the interacting epitope map of the interaction between tRha-LPS and DC-SIGN derived from STD NMR data and computational studies (left) and most representative NOE values to determine the bioactive conformation (right). (D) tr-ROESY NMR on the 1:30 mixture of DC-SIGN:tRha-LPS. (E) Schematic representation of the bioactive conformation with the core oligosaccharide sugars colored in according to the SNFG nomenclature and the OPS sugars in gray.

5-Mer **6** (in 77 and 54% yields, respectively). Global deprotection of 3-Mer **3** and 5-Mer **6** via Pd-catalyzed hydrogenolysis, Zemplén methanolysis, and CAN oxidation led to the removal of all the protecting groups to provide the desired rhamnose-terminated 3-Mer **4** and 5-Mer **7** (see the Supporting Information for details).

These *ad hoc* synthesized oligomers bearing L-Rha as the terminal moiety (3-Mer and 5-Mer) were therefore studied for their interaction with DC-SIGN, following the same approach as above. Interestingly, NMR and biophysical studies detected no binding with DC-SIGN (see Figure S9 and Discussion below). The absence of recognition was further proved by NMR experiments, as upon addition of D-mannose (in the same 1:30 ratio) to the sample, it was possible to observe the presence of STD NMR signals deriving from the monosaccharide and showing that there was no interaction with both 3-Mer and 5-Mer and that the protein was still functional (data not shown).

BVMPK LPS O-Antigen–DC-SIGN: Surface Plasmon Resonance Analysis

Surface plasmon resonance (SPR) experiments were performed to further validate the proposed 3D system. Thus, oligomers containing from one to eight repeating units (2-Mer, 4-Mer, 8-Mer, and 16-Mer) were used in an SPR competition

https://doi.org/10.1021/jacsau.3c00748
JACS Au 2024, 4, 697−712

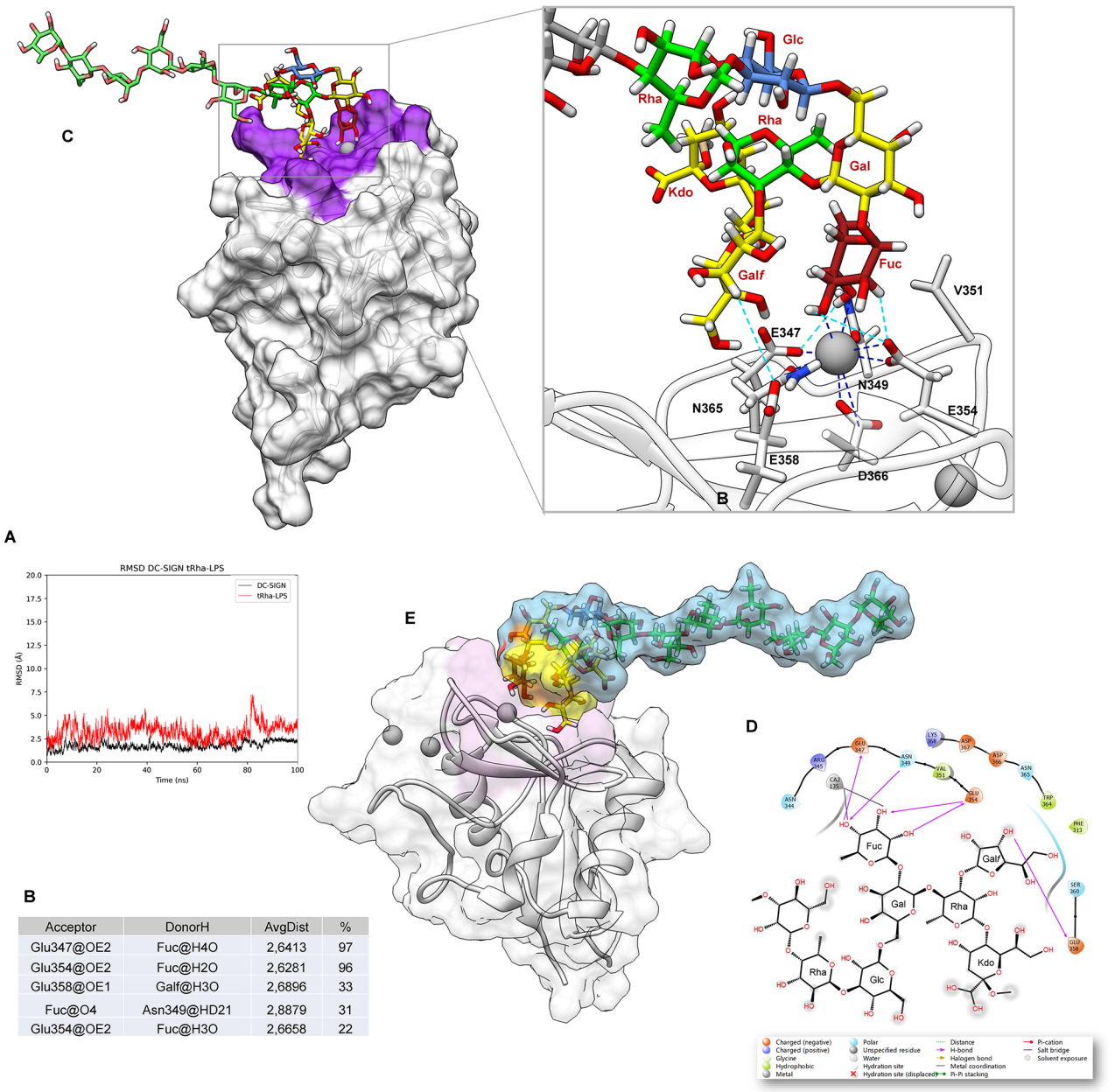

B

Acceptor	DonorH	AvgDist	%
Glu347@OE2	Fuc@H4O	2,6413	97
Glu354@OE2	Fuc@H2O	2,6281	96
Glu358@OE1	Galf@H3O	2,6896	33
Fuc@O4	Asn349@HD21	2,8879	31
Glu354@OE2	Fuc@H3O	2,6658	22

Figure 7. DC-SIGN: tRha-LPS complex MD simulation analysis. (A) RMSD of the protein (black) and ligand (red) being the ligand RMSD calculated in reference to the protein. (B) Protein−ligand H-bonds described as acceptor, donor, distance, and stability (in percentage) during the 100 ns MD simulation. (C) 3D model of the DC-SIGN−tRha-LPS complex with the protein amino acids involved in the interaction highlighted in purple. Close-up view of a representative pose from the most populated MD family. In gray, the Ca^{2+} ions. The ligand is colored according to SNFG nomenclature. Ca^{2+} coordination bonds are shown as dashed blue lines, while the observed H-bond interactions are indicated by dashed cyan lines. (D) Two-dimensional plot representation of the most stable interactions between tRha-LPS and DC-SIGN binding pocket residues. (E) 3D representation of the DC-SIGN: tRha-LPS complex with the ligand surface colored according to the STD NMR results.

test to evaluate their affinity toward DC-SIGN (Figure 5 and Figures S10−S19).[34]

Independent of the size of the oligomer tested, the IC_{50} determined were in the same range, between 3 and 4.2 mM (Table 1), and did not change significantly from 2-Mer to 16-Mer. Considering the increase in repeating units, the results showed that the main contribution to the binding was entirely contained within the terminal unit. Additional units on the reducing end did not significantly improve the competitive power of the oligomers in the test and, thus, the binding affinity to the DC-SIGN binding site. Moreover, the IC_{50} value obtained here for 2-Mer was of 3.3 mM, which is almost identical to the one classically obtained for a single mannose in this competition test (around 3 mM),[35] thus supporting the key role of the tMan that accounts for almost all of the binding energy. This experimental evaluation of the affinity further supported the NMR experiments and MD calculation.

B. vulgatus Full Core LPS−DC-SIGN Binding Studies

The presence in *B. vulgatus* core LPS of uncommon sugars like Fuc (fucose) and Galf (galactofuranose) increased our interest in unveiling their interaction with DC-SIGN. To this aim, the full LPS containing three OPS repeating units (terminating with a Rha residue) and the full core heptasaccharide starting

https://doi.org/10.1021/jacsau.3c00748
JACS Au 2024, 4, 697−712

from Kdo (Figure 6)[36] were investigated. STD NMR experiments and the corresponding binding epitope on BVMPK LPS, containing the full core and three OPS repeating units (with a tRha as a terminal residue, tRha-LPS, Figures 6 and 7), supported the above findings and confirmed how the OPS portion containing the terminal tRha did not interact with the protein. As for the core region, the fucose unit was, as expected, the main sugar accommodated in the protein binding site; interestingly, also the Gal*f* residue was significantly involved (Figure 6B,C, see below) and Gal and Kdo units were also located nearby the protein surface (see Figure 6 and Figure S20). In detail, the STD-derived interacting epitope revealed how the recognition took place mainly through the Fuc unit, with strongest effects ascribed to H1 to H4 protons (above 70%), and in addition almost all Gal*f* protons, mainly the H2 Gal proton and the side chain protons of Kdo (H6, H7, and H8), gave moderate to good STD signals. These results also highlighted the proximity to the binding pocket of Gal, Gal*f*, and Kdo; likely, the rest of the core was solvent exposed. The evaluation of the bioactive conformation of the tRha-LPS, inferred by tr-ROESY NMR experiments run on the DC-SIGN: tRha-LPS system (Figure 6C), allowed us to further detail the conformational features of the interaction. As previously discussed, the key *inter*-proton distances were derived from trNOE experiments and were used to evaluate the conformational behavior of tRha-LPS in the bound state (see the Supporting Information and Table S3).

In order to depict a 3D model of tRha-LPS in the DC-SIGN binding pocket via MD simulations, the uncommon sugars of the inner core region, such as Gal*f* and Kdo, were first and successfully parametrized using the AMBER18 package.[37] Then, the disaccharides constituting the core region were built to evaluate the energetically accessible conformational regions via MM calculations using standard protocols (see the experimental section, Molecular Mechanics and Molecular Dynamics Simulation section). The adiabatic energy maps, which illustrate the ϕ/ψ and ϕ/ω glycosidic torsion angles (Figure S21), confirmed that the global energy minimum aligned with the *exo*-anomeric effect. Thus, the tRha-LPS tridecasaccharide in its bioactive conformation was manually docked into the DC-SIGN binding site using PDB 1SL5 as the template,[38] to run the MD simulation. RMSD calculations conducted on both protein backbone and ligand residues, using the first frame as a reference, provided evidence of complex stability (Figure 7). The glycosidic torsion angles were sampled during the MD simulations in both free and bound states (trajectories and $\phi/\psi-\phi/\omega$ scatter plots of the glycosidic linkages are shown in Figures S22 and S23), to assess the conformational behavior. The corresponding average distances obtained for the simulation from $\langle r^{-6}\rangle$ values were compared to those collected experimentally obtained, and an excellent accordance was found (Figures S20C−S24 and Table S3). MD results showed that the torsion angles mainly adopted values in accordance with the *exo*-syn anomeric conformation and confirmed how the Gal*f* residue pointed close to the Fuc unit, as inferred by the *inter*-residue NOE contacts (such as G5-H3; see Figure 7), and consequently was located close to the protein surface. Furthermore, the Fuc residue was accommodated in the protein binding site and acted as an anchor, establishing key interactions with DC-SIGN and stabilizing the whole ligand by coordination with the Ca^{2+} ion in the canonical way, through hydroxyl moieties at positions 3 and 4 (Figure 6). Additionally, the Fuc residue was stabilized by further H-bond interactions, with hydroxyl moieties at positions 2, 3, and 4 establishing strong interactions with DC-SIGN. The most stable interaction was observed between Fuc 4-OH as a H-bond donor with E347 (97% of the MD, Figure 7) and as a H-bond acceptor with N349 (31%); E354 was found as a H-bond acceptor in both the interaction with 2-OH (96%) and 3-OH (22%). In addition, the conformation adopted by tRha-LPS supported the location of Gal*f* close to the binding pocket in the 3D complex, as confirmed by both STD and trNOE data. Interestingly, MD simulation also proved that Gal*f* 3-OH acted as a H-bond donor to E358 (Figure 7) and that the conformational features of tRha-LPS also moved H6, H7, and H8 Kdo close to the binding pocket, supporting the experimental STD effects. Furthermore, CORCEMA-ST analysis was also run on the DC-SIGN: tRha-LPS complex, finding a good agreement between the experimental and the predicted calculations (Figure S25). Hence, computational results fully matched and integrated NMR data and provided information on the further accommodation of *Bacteroides* core LPS inside DC-SIGN binding pocket (see Figures 6 and 7 and Discussion for more details).

DISCUSSION

The interest in studying the role and host immune perception of bacterial envelope glycoconjugates has dramatically increased given their ability to act as MAMPs triggering host immune response.[8,39−41] The open questions are still many and yet to be fully addressed especially in the context of GM and its modulation of the host immune system.[22] The host's ability to discriminate beneficial and harmful species implies that commensal bacteria express chemically distinct MAMPs that differently modulate the immune response. LPS-driven immune activation is strongly structure-dependent and ranges from a potent to moderate stimulation to the inhibition of the immune response in antagonistic LPS.[42]

A wide range of CTLs, located on the plasma membrane of antigen-presenting cells, constitutes an important family of antigen uptake membrane receptors; the sensing of commensals by host lectins is likely to promote host−microbiota mutualism, preventing systemic inflammation.[43] Syk-coupled CTL Mincle is expressed in Peyer's patches which, after stimuli from commensal bacteria, trigger IL-6 and IL-23p19 expression, regulating the function of intestinal Th17- and IL-17-secreting ILCs, with the consequent production of IgA. CTL receptor DC-SIGN fulfills a large number of immune-related functions, mainly related to antigen uptake, processing, and immune regulation, and acts as an immune homeostatic receptor, since its interaction with host ligands can trigger anti-inflammatory responses. Ligand recognition mediates both internalization and signaling. Furthermore, DC-SIGN-dependent cross-presentation is enhanced by the simultaneous triggering of TLRs, being described as its ability to modify TLR signaling in a pro- or anti-inflammatory way depending on the ligand recognized.[44,45]

The dual role in mediating both tolerance and immune response, depending on the context, might have been exploited by pathogens and tumors that upregulate the expression of DC-SIGN ligands to take advantage of DC-SIGN-dependent tolerogenic signaling as a strategy to escape the immune system.[18,44] DC-SIGN preferentially binds to fucosylated glycans, such as blood-type Lewis antigens (Le^a, Le^b, Le^X, Le^Y, and sulfo-Le^a)[46] and mannose-exposing ligands, which

https://doi.org/10.1021/jacsau.3c00748
JACS Au 2024, 4, 697−712

stimulates the TLR-induced cytokine response. Both mannose and fucose ligands stimulate IL-10 secretion, but while fucosylated ligands reduce LPS-induced IL-6 and IL-12 secretion, Man ligands increase the production of both interleukins. This attributed an anti-inflammatory response to fucose-expressing ligands and a pro-inflammatory response to the mannose-expressing ones.[47] Nevertheless, in the last decades, DC-SIGN's ability to recognize GlcNAc or Gal residues among others has been proved.[31,38,48−51] Indeed, we recently proved that DC-SIGN binds to the *E. coli* R1 core oligosaccharide by recognizing its outer core pentasaccharide, which acts as a cross-linker between two tetrameric units of DC-SIGN.[52] This discovery further enhances the understanding of the DC-SIGN interaction with LPS and offers the potential for the development of strategies to prevent and treat bacterial infections through pharmacological and immunostimulatory means.

Here, by an intertwined interdisciplinary approach, organic synthesis efforts complemented with NMR, computational, and biophysical studies were employed to propose a 3D complex of the interaction between DC-SIGN and *B. vulgatus* mpk (BVMPK) LPS (Figures 3, 4, 6, and 7). This molecular glance can certainly furnish relevant information for in vivo *B. vulgatus* LPS immune recognition and the role exerted by its sugar moieties; furthermore, the knowledge at the atomic level of LPS recognition by DC-SIGN can open new avenues toward its therapeutic use against GM-related inflammatory diseases. Indeed, we show how the interaction between DC-SIGN and BVMPK LPS O-antigen takes place by its terminal portion, and it is not length dependent but instead sugar dependent; in fact, the elongation of the chain does not affect the recognition and binding process whereas the presence of a terminal Man residue is crucial in the recognition and binding process. We have shown this by conducting binding studies on Rhamnose terminating 3-Mer and 5-Mer oligomers, which showed no interaction with DC-SIGN, and confirmed on the tRha-LPS. This pointed out the importance of the biological repeating unit of *B. vulgatus* LPS O-antigen in dictating the interaction with host lectins. Computational studies further defined the binding process, indicating how, for all oligomers, the interaction occurred through the terminal disaccharide moiety (tMan-Rha) while the rest of the ligand remains solvent exposed instead of being smeared on top of the protein. In all MD studies, the oligomers maintain coordination with the principal Ca^{2+} atom through tMan hydroxyl moieties in positions 3 and 4 (Figures 3 and 4). In addition to the above findings, our analysis also reveals two different binding modes, **BmA** and **BmB**, as a result of the 180° rotation through the tMan residue inside the binding site, which were observed and analyzed in this study. **BmA** represented the predominant binding mode, while **BmB** contributed approximately 30% of the ensemble weight. The coexistence of these binding modes underscores the complexity of the binding process and highlights the dynamic nature of the interaction between BVMPK O-antigen and DC-SIGN. Indeed, CORCEMA-ST results not only aided validating the optimal 3D model for the protein−ligand complexes but also highlighted the critical role of the terminal mannose (tMan) in the interaction, with particular emphasis on the contributions of H3 and H4, which were predicted to have the strongest STD values, in agreement with experimental NMR results. These results not only enhance our understanding of the molecular interactions but also have important implications for elucidating the underlying binding mechanisms.

The combination of spectroscopic and computational studies also unveiled the bioactive (bound) conformation of tRha-LPS, showing how the BVMPK LPS core region interacted with DC-SIGN and highlighting the key residues involved in the binding process. Indeed, binding studies performed on the *ad hoc* synthesized tRha-LPS revealed that Fuc and the directly linked Gal residues, but also Gal*f* and Kdo moieties, were involved in LPS core recognition by DC-SIGN (Figures 6 and 7). Specifically, the Fuc residue was crucial in the interaction, being located in the protein binding site and acting as anchor; Fuc coordinates the primary Ca^{2+} ion through 3OH and 4OH while also establishing stable H-bonds with E347 and N349 through 4OH and with E354 through hydroxyl moieties at positions 2 and 3. Moreover, Gal and Gal*f* and in minor amounts Kdo residues were also near the binding pocket while most of the core and the OPS were solvent exposed. Notably, only the flexible side chain of Kdo interacted with DC-SIGN while no contribution from the sugar ring protons was detected. This likely keeps the lipid A moiety far from the protein surface and facilitates the interaction of the whole LPS moiety with DC-SIGN, avoiding steric hindrances either in the monomeric or in the tetrameric form (Figure S26). Moreover, Rhamnose is an ubiquitous sugar found in a diverse array of microbial species, including *Shigella*, *Pseudomonas*, *Campylobacter*, and *Streptococcus*, underscoring the complexity of its role in bacterial virulence and pathogenesis. The impact of rhamnose on these processes is not uniform across different species; rather, it is deeply context-dependent and intricately linked with a multitude of other bacterial and host factors. Such factors include the overall composition of the O-antigen, the presence of other virulence determinants in the bacterium, and the nature of the host immune response. Therefore, while rhamnose is a common component of O-antigens, its presence alone does not straightforwardly correlate with increased virulence or pathogenicity. Instead, its role must be considered within the broader and more complex landscape of microbial−host interactions.

Therefore, we can here describe a novel, complex exogenous (bacterial) binding epitope for DC-SIGN involving the *B. vulgatus* core and the O-antigen LPS portion: a terminal β-Man linked to an internal, L-configured Rhamnose residue and a terminal α-Fucose located in the inner core region. The recognition of the Fuc moiety in the inner core region is also supported by DC-SIGN preference for Fuc over Man.[53] Considering that fucose and mannose residues in BVMPK LPS are recognized by DC-SIGN, we can hypothesize that *B. vulgatus* LPS contributes to the establishment of homeostasis by interacting with DC-SIGN and inducing a controlled host response. Moreover, we can also structurally hypothesize an LPS-mediated bivalent bridge favoring the binding to CRDs from two different DC-SIGN tetramers, where one DC-SIGN tetramer is involved in the interaction with the O-antigen portion while another establishes interactions with the core oligosaccharide through the fucose unit (Figure S26). This mechanism would surely benefit BVMPK LPS in the hunting for DC-SIGN because of its superior ability, i.e., a double bait. Additionally, we have recently shown how the chelate binding mode (two interactions in two adjacent CRD of a similar DC-SIGN tetramer) can drastically increase the strength of interaction through an avidity mechanism.[54] Moreover, in

https://doi.org/10.1021/jacsau.3c00748
JACS Au 2024, 4, 697−712

addition to this internal avidity at the level of one DC-SIGN receptor, we can straightforwardly imagine clustering of DC-SIGN receptors generated in the context of interaction with the LPS exposed at the bacterial surface. Indeed, Jarvis et al.[55] proved that receptor clustering affects the efficiency of antigen internalization, as the longer is the ligand the greater is the extent of internalization to endosomal compartments that lead to antigen processing.

CONCLUSIONS

CTLs like DC-SIGN have a key role in microbial recognition and immunity; viruses like HIV have developed mechanisms to co-opt lectins for dissemination instead of following traditional endocytic pathways or being degraded.[55,56] Bacterial carbohydrate-specific signaling by DC-SIGN can modulate TLR-mediated responses and tailor adaptive immune responses to specific pathogens. However, it has been unclear whether and how DC-SIGN interacts with carbohydrates expressed by the microbiota and how this affects immunity. We here provide a very reasonable working hypothesis on the mechanism of binding based on a heterobivalent recognition of two different carbohydrate regions; i.e., a safe recognition with a double check would surely benefit DC-SIGN recognition by this LPS in competition with a multitude of microbial glycan, even pathogenic ones. In conclusion, this work provides a first insight at the molecular level into the direct role of *B. vulgatus* LPS in the immunomodulation of the host, concurrently important to delineate the key molecules underlying host–microbiota interactions.

METHODS

NMR Analysis

The NMR experiments were recorded on a Bruker AVANCE NEO 600-MHz equipped with a cryo probe, and data acquisition and processing were performed with TopSpin 4.1.1 software. Samples were prepared in 50 mM buffered phosphate at pH 7.4, using 3 mm NMR tubes. NMR binding experiments were run by using a protein ECD concentration of 20 μM. For STD NMR analysis, STD NMR experiments were acquired with 32,000 data points and zero-filled up to 64,000 data points prior to processing. The protein ECD resonances were selectively irradiated using 40 G pulses with a length of 50 ms, setting the off-resonance pulse frequency at 40 ppm and the on-resonance pulses at 6.5 and 7.5 ppm. An excitation sculpting with gradient pulses (esgp) was applied for the suppression of water signals. The %STD displayed in the ligands' epitope maps were obtained by the ratio of the STD signals in the STD spectra ($I_0 - I_{sat}$) and each relative peak intensity of the unsaturated reference spectrum (off-resonance, I_0), at saturation time of 2 s. The highest STD signal was set to 100%, and all the other STD values were normalized to this value. For tr-NOESY analysis, homonuclear 2D NOESY experiments were conducted by using data sets of 4096 × 900 points and mixing times of 100–400 ms. The interproton cross relaxation rates (σ_{ij}) were measured by the integration of the NOE cross peaks of interest and normalizing against the corresponding cross peak on the diagonal in F1. The experimental distances (r_{ij}) were then obtained by employing the isolated spin pair approximation. For Carr–Purcell–Meiboom–Gill, the cpmgz pulse program based on the spin–echo pulse sequence was used for the acquisition of the CPMG experiment. The signal relaxation was measured for 100 ms, and the experiment was acquired with 256 scans. The recycle delay was set to 2 s, and a fixed echo time was chosen at 3 ms. STD NMR experiments in the presence of 20 mM EDTA-d12 were performed in order to chelate all available divalent Ca^{2+} ions.

Molecular Mechanics and Molecular Dynamics Simulation

Molecular mechanics calculations were performed using the MM3* force field in the vacuum, and a dielectric constant of 80 was used. For the disaccharide structure, both Φ and Ψ were varied incrementally using a grid step of 18°; each (Φ, Ψ) point of the map was optimized using 2000 P.R. Molecular dynamics calculations were performed with AMBER 18 software[37] in explicit waters using AMBER ff14SB, Glycam06j-1, and TIP3P force fields for the protein residues, the saccharide ligand, and the water solvent molecules, respectively. The different ligands were downloaded from the GLYCAM web site (www.GLYCAM.org).[57] In order to prepare the protein, missing hydrogen atoms were added and protonation states of ionizable groups and cap termini were computed by using Maestro Protein Preparation Wizard.[58] The different systems followed the same protocol, being hydrated with an octahedral box containing the explicit TIP3P water molecules buffered at 15 Å and also adding counterions to neutralize the system. The input files were generated by using the tleap modules of the AMBER package. The Sander module was used for the minimization steps, while molecular dynamic calculations were performed using the PMEMD module. At this point, an energy minimization process was performed to refine the initial structure. The calculations employed SHAKE for the C–H bonds and 1 fs of the integration step. Periodic boundary conditions were applied as well as the smooth particle mesh Ewald method to represent the electrostatic interactions, with a grid space of 1 Å. At first, the system was minimized holding the complex while a further minimization step was performed on the entire system. Subsequently, the whole system was slowly heated from 0 to 300 K by applying a weak restraint on the solute. Temperature was increased from 0 to 100 K at constant volume and then from 100 to 300 K in an isobaric ensemble. Thereafter, the temperature was kept constant at 300 K during 50 ps with progressive energy minimizations and solute restraint. Upon completion of the equilibration, the system restraints were removed and the systems then advanced in an isothermal–isobaric ensemble along the production. The system coordinates were saved and used for the 100 ns simulations using the PMEMD module implemented in AMBER. Coordinate trajectories were recorded each 2 ps throughout production runs, yielding an ensemble of 10,000 structures for each complex, which were finally analyzed. In the specific case of the tRha-LPS:DC-SIGN complex, a restraint was applied to the Rha-Glc torsion in order to avoid the population of the non-exo conformation. The non-parametrized residues (Kdo and Galf) were parametrized using a self-made protocol performing the Restrained Electrostatic Potential (RESP) charge calculation with a Hartree–Fock calculation and a 6-31G* basis set. Antechamber and xLeap were combined to generate the .prep and .frcmod files.[59] Trajectories were analyzed using the ptraj module within AMBER 18, and the VMD[60] program was used to visualize the MD results. Each trajectory was submitted to cluster analysis with respect to the ligand RMSD using the K-mean algorithm implemented in the ptraj module. The representative structure of the most populated cluster was considered to depict the complexes interactions. The determination of hydrogen bonds was calculated using the CPPTAJ module in AMBER 18.[59] The h-bond is defined as occurring between an acceptor heavy atom A, a donor hydrogen atom H, and a donor heavy atom D. The distance cutoff was set to 3 Å, and the A-H-D angle cutoff was 135°. The 3D images shown have been prepared with the USCF Chimera program.[61] Dihedral conformation analysis has been performed using a homemade script to depict the variation of the torsion during the MD simulation and obtain an histogram of the most populated values

ELISA Experiments

50 μL from a 25 μg/mL *B. vulgatus* LPS solution (dissolved in PBS 10 mM, pH = 7.4) was used to coat NUNC MaxiSorp ELISA wells (for 2 h at room temperature). After discarding and washing with the calcium and magnesium-containing buffer TSM [20 mM tris-(hydroxymethyl)aminomethane (Tris)-HCl, pH 8.0; 150 mM NaCl; 1 mM $CaCl_2$; 2 mM $MgCl_2$] (1 × 150 μL), wells were blocked with a TSM solution with 1% BSA (100 μL, Sigma-Aldrich, ≥96%, agarose gel electrophoresis) at room temperature for 30 min.

https://doi.org/10.1021/jacsau.3c00748
JACS Au 2024, 4, 697–712

The blocking solution was discarded followed by the addition of 50 μL of DC-SIGN-Fc at 25 μg/mL (alone or preincubated for 1 h with serial dilutions of LPS from *B. vulgatus*), in TSM with 0.5% BSA. After 1 h at room temperature, wells were washed with TSM (2 × 150 μL) followed by the addition of 100 μL of antihuman horseradish peroxidase (0.8 μg/mL, Life Technologies, Goat Anti-Human IgG-HRP). After 30 min at room temperature, wells were washed with TSM (2 × 150 μL) and 100 μL of substrate solution (3,3′,5,5′-tetramethylbenzidine, TMB, citric/acetate buffer, pH = 4, plus H_2O_2) were added. After 3 min of incubation at room temperature, the colorimetric reaction was stopped with 50 μL of 0.8 M of H_2SO_4. The optical density (OD) was measured at 450 nm in an ELISA reader. Data were normalized over the signal at 450 nm from the BSA-containing wells.

CORCEMA-ST

The CORCEMA-ST protocol, as previously described by Jayalakshmi and Krishna,[30] was employed. The coordinates for the complexes were chosen from MD trajectory analyses. It was assumed, as observed by NMR, that the ligand's conformation remained constant between the free and bound states. The input parameters, such as ligand and protein concentrations, were determined experimentally. A saturation time of 2 s was set, and the dissociation constants (KD) were initially determined based on experimental data for the DC-SIGN/4-Mer and DC-SIGN/tRha-LPS complex, with further adjustments to achieve the best fit. A binding-site cutoff of 6 Å was applied. Fractional intensity changes for each ligand proton were calculated by computing the R matrix and spectral densities. These changes were then compared to the experimental STD effects using the NOE R factor, a normalized root-mean-square deviation value. In these calculations, only the STD values of the ligand's isolated signals were considered.

Surface Plasmon Resonance (SPR) Analysis

DC-SIGN ECD used for the SPR competition assay was produced as previously described in Tabarani et al.[62] The SPR competition experiments were performed on a Biacore T200 using a CM3 sensor chip. Flow cells were activated as previously described.[63] Flow cell 1 was functionalized with BSA, blocked with ethanolamine, and subsequently used as a control surface. Flow cells 2 and 3 were treated with BSA-Manα1−3[Manα1−6]Man (Dextra) (60 μg/mL) in 10 mM NaOAc pH 4 to reach different binding densities and blocked with ethanolamine. The final densities on flow cells 2 and 3 were 2690 and 1715 RU, respectively. The use of these two-flow cells allows redundancy in the measurements. The affinity of the different oligomers of repeating units (from 2-Mer to 16-Mer) for the DC-SIGN extracellular domain (ECD) was evaluated via an established inhibition assay[64] in which DC-SIGN ECD was injected at 20 μM alone or in the presence of increasing concentration of oligomers (ranging from 20 mM to 40 μM of the corresponding oligomer obtained by serial dilution by a factor of 2). Injections were performed at 5 μL/min using 25 mM Tris−HCl pH 8, 150 mM NaCl, 3.8 mM $CaCl_2$, and 0.05% P20 surfactant as running buffer. The surface was regenerated by the injection of 50 mM EDTA. DC-SIGN ECD equilibrium binding responses (R_{eq}) for each sample were obtained from the reference surface corrected sensorgrams 95 s after the start of the injection. The obtained R_{eq} values were converted to DC-SIGN residual activity values (y, %) with respect to R_{eq} of DC-SIGN alone, which was assigned a 100% activity value. After plotting residual activity against corresponding compound concentration, the 4-parameter logistic model (eq 1) was fitted to the plots and the IC_{50} values were calculated using eq 2.

$$y = R_{hi} - \frac{R_{hi} - R_{lo}}{1 + \left(\frac{Conc}{A_1}\right)^{A_2}} \quad (1)$$

$$IC_{50} = A_1 \times \left(\frac{R_{hi} - R_{lo}}{R_{hi} - 50}\right)^{\frac{1}{A_2}} \quad (2)$$

where R_{hi} and R_{lo} are the maximum and minimum asymptotes, respectively, A1 is the inflection point, and A2 is a slope of the curve.

ASSOCIATED CONTENT

Supporting Information

The Supporting Information is available free of charge at https://pubs.acs.org/doi/10.1021/jacsau.3c00748.

Synthesis of *B. vulgatus* OPS repeating units; experimental procedures; supporting text, figures, and tables; interproton distances; CORCEMA-ST results; NMR and MD derived figures; and SPR spectra (PDF)

Figures S1−S26 (PDF)

Figures S27−32 (PDF)

AUTHOR INFORMATION

Corresponding Authors

Biao Yu − *State Key Laboratory of Bioorganic and Natural Products Chemistry, Shanghai Institute of Organic Chemistry, University of Chinese Academy of Sciences, Chinese Academy of Sciences, Shanghai 200032, China;* orcid.org/0000-0002-3607-578X; Email: byu@sioc.ac.cn

Alba Silipo − *Department of Chemical Sciences, University of Naples Federico II, Naples 80126, Italy;* orcid.org/0000-0002-5394-6532; Email: silipo@unina.it

Authors

Ferran Nieto-Fabregat − *Department of Chemical Sciences, University of Naples Federico II, Naples 80126, Italy;* orcid.org/0000-0001-9847-3030

Qian Zhu − *State Key Laboratory of Bioorganic and Natural Products Chemistry, Shanghai Institute of Organic Chemistry, University of Chinese Academy of Sciences, Chinese Academy of Sciences, Shanghai 200032, China*

Corinne Vivès − *Université Grenoble Alpes, CNRS, CEA, Institut de Biologie Structurale, Grenoble 38027, France*

Yunqin Zhang − *State Key Laboratory of Phytochemistry and Plant Resources in West China, Kunming Institute of Botany, University of Chinese Academy of Sciences, Chinese Academy of Sciences, Kunming 650201, China*

Angela Marseglia − *Department of Chemical Sciences, University of Naples Federico II, Naples 80126, Italy;* orcid.org/0000-0003-1831-6831

Fabrizio Chiodo − *Institute of Biomolecular Chemistry, National Research Council (CNR), Pozzuoli 80078, Italy*

Michel Thépaut − *Université Grenoble Alpes, CNRS, CEA, Institut de Biologie Structurale, Grenoble 38027, France*

Diksha Rai − *Department of Chemistry, Indian Institute of Technology Bombay, Mumbai 400076, India*

Suvarn S. Kulkarni − *Department of Chemistry, Indian Institute of Technology Bombay, Mumbai 400076, India;* orcid.org/0000-0003-2884-876X

Flaviana Di Lorenzo − *Department of Chemical Sciences, University of Naples Federico II, Naples 80126, Italy*

Antonio Molinaro − *Department of Chemical Sciences, University of Naples Federico II, Naples 80126, Italy;* orcid.org/0000-0002-3456-7369

Roberta Marchetti − *Department of Chemical Sciences, University of Naples Federico II, Naples 80126, Italy;* orcid.org/0000-0002-7173-7099

Franck Fieschi − *Université Grenoble Alpes, CNRS, CEA, Institut de Biologie Structurale, Grenoble 38027, France;*

Institut Universitaire de France (IUF), Paris 75005, France; orcid.org/0000-0003-1194-8107

Guozhi Xiao − *State Key Laboratory of Phytochemistry and Plant Resources in West China, Kunming Institute of Botany, University of Chinese Academy of Sciences, Chinese Academy of Sciences, Kunming 650201, China;* orcid.org/0000-0002-4724-4390

Complete contact information is available at: https://pubs.acs.org/10.1021/jacsau.3c00748

Author Contributions

A.S. conceived the study. A.S. and B.Y. designed the research. All the authors executed the research and have given approval to the final version of the manuscript. CRediT: **Ferran Nieto-Fabregat** data curation, formal analysis, investigation, methodology, software, visualization, writing-original draft; **Qian Zhu** data curation, formal analysis, investigation, writing-original draft; **Corinne Vivès** data curation, formal analysis, methodology; **Yunqin Zhang** data curation, formal analysis, investigation; **Angela Marseglia** formal analysis; **Fabrizio Chiodo** formal analysis, investigation; **Michel Thépaut** formal analysis, investigation; **DIKSHA RAI** investigation; **Suvarn S. Kulkarni** investigation; **Flaviana Di Lorenzo** data curation, formal analysis, funding acquisition, writing-original draft; **Antonio Molinaro** data curation, funding acquisition, writing-original draft; **Roberta Marchetti** data curation, funding acquisition, investigation, methodology, supervision, writing-original draft, writing-review & editing; **Franck FIESCHI** data curation, formal analysis, investigation, writing-original draft; **Guozhi Xiao** data curation, investigation, writing-original draft; **Biao Yu** conceptualization, funding acquisition, investigation, writing-original draft, writing-review & editing; **Alba Silipo** conceptualization, data curation, funding acquisition, investigation, project administration, supervision, writing-original draft, writing-review & editing.

Notes

The authors declare no competing financial interest.

ACKNOWLEDGMENTS

This study was supported by PRIN 2017 (2017XZ2ZBK, 2019-2023) and PRIN PNRR 2022 P2022M457Z to A.S.; by the European Research Council (ERC) under the European Union's Horizon 2020 research and innovation program under grant agreement No 851356 to R.M.; and by the ERC under the Horizon Europe grant agreement no. 101039841 to F.D.L. The European Union (FSE, PON Ricerca e Innovazione 2014−2020, Azione I.1 'Dottorati Innovativi con caratterizzazione Industriale') is acknowledged for funding the Ph.D. grant to A.Ma.; FN-F. and A.Mo. acknowledge H2020-MSCA-ITN-2018 (SweetCrossTalk) grant agreement 814102 and PRIN 2020 2020BKK3W9. This work is financially supported by the National Key Research & Development Program of China (2018YFA0507602), the Key Research Program of Frontier Sciences of the Chinese Academy of Sciences (ZDBS-LY-SLH030), and the Shanghai Municipal Science and Technology Major Project. S.S.K. thanks the Science and Education Research Board (Grant Nos. CRG/2019/000025 and SPR/2021/000328) and CSIR (Grant No. 02(0413)/21/EMR-II) for the financial support. D.R. thanks the Department of Science and Technology for DST-Inspire fellowships. This work used the platforms of the Grenoble Instruct-ERIC centre (ISBG; UAR 3518 CNRS-CEA-UGA-EMBL) within the Grenoble Partnership for Structural Biology (PSB), supported by FRISBI (ANR-10-INBS-0005-02) and GRAL, financed within the University Grenoble Alpes Graduate School (Ecoles Universitaires de Recherche) CBH-EUR-GS (ANR-17-EURE-0003). F.F. also acknowledges the French Agence Nationale de la Recherche (ANR) PIA for Glyco@Alps (ANR-15-IDEX-02) and ANR PRCI LectArray 19-CE18-0019-01. A.S. and R.M. acknowledge PNRR, Missione 4 − Componente 2 − NextGenerationEU - Partenariato Esteso INF-ACT - One Health Basic and Translational Research Actions Addressing Unmet Needs on Emerging Infectious Diseases MUR: PE00000007.

ABBREVIATIONS

CTL, C-type lectin; BVMPK, *Bacteroides vulgatus* mpk; GM, gut microbiota; LPS, lipopolysaccharide; CRD, carbohydrate-recognition domain; DC-SIGN, dendritic cell-specific intracellular adhesion molecules (ICAM)-3 grabbing nonintegrin; SPR, surface plasmon resonance

REFERENCES

(1) de Vos, W. M.; Tilg, H.; Van Hul, M.; Cani, P. D. Gut microbiome and health: Mechanistic insights. *Gut* **2022**, *71* (5), 1020−1032.

(2) Pandey, S.; Kawai, T.; Akira, S. Microbial sensing by Toll-like receptors and intracellular nucleic acid sensors. *Cold Spring Harb. Perspect. Biol.* **2015**, *7* (1), No. a016246.

(3) Takeuchi, O.; Akira, S. Pattern recognition receptors and inflammation. *Cell* **2010**, *140* (6), 805−820.

(4) Di Lorenzo, F.; Duda, K. A.; Lanzetta, R.; Silipo, A.; De Castro, C.; Molinaro, A. A Journey from Structure to Function of Bacterial Lipopolysaccharides. *Chem. Rev.* **2022**, *122* (20), 15767−15821.

(5) Steimle, A.; Michaelis, L.; Di Lorenzo, F.; Kliem, T.; Munzner, T.; Maerz, J. K.; Schafer, A.; Lange, A.; Parusel, R.; Gronbach, K.; Fuchs, K.; Silipo, A.; Oz, H. H.; Pichler, B. J.; Autenrieth, I. B.; Molinaro, A.; Frick, J. S. Weak Agonistic LPS Restores Intestinal Immune Homeostasis. *Mol. Ther.* **2019**, *27* (11), 1974−1991.

(6) Mohr, A. E.; Crawford, M.; Jasbi, P.; Fessler, S.; Sweazea, K. L. Lipopolysaccharide and the gut microbiota: considering structural variation. *FEBS Lett.* **2022**, *596* (7), 849−875.

(7) Di Lorenzo, F.; De Castro, C.; Lanzetta, R.; Parrilli, M.; Silipo, A.; Molinaro, A.; Jimenez-Barbero, J.; Canada, F. J.; Martin-Santamaria, S. Lipopolysaccharides as microbe-associated molecular patterns: a structural perspective. *Carbohydr. Drug Des. Discovery* **2015**, *ch. 3*, 38−63.

(8) Brown, G. D.; Willment, J. A.; Whitehead, L. C-type Lectins in immunity and homeostasis. *Nat. Rev. Immunol.* **2018**, *18* (6), 374−389.

(9) Napoletano, C.; Zizzari, I. G.; Rughetti, A.; Rahimi, H.; Irimura, T.; Clausen, H.; Wandall, H. H.; Belleudi, F.; Bellati, F.; Pierelli, L.; Frati, L.; Nuti, M. Targeting of macrophage galactose-type C-type lectin (MGL) induces DC signaling and activation. *Eur. J. Immunol.* **2012**, *42* (4), 936−945.

(10) Kalograiaki, I.; Euba, B.; Fernández-Alonso, M. D. C.; Proverbio, D.; St. Geme, J. W.; Aastrup, T.; Garmendia, J.; Cañada, F. J.; Solís, D. Differential recognition of Haemophilus influenzae whole bacterial cells and isolated lipooligosaccharides by galactose-specific Lectins. *Sci. Rep.* **2018**, *8* (1), 1−12.

(11) Singh, S.; Almuhanna, Y.; Alshahrani, M. Y.; Lowman, D. W.; Rice, P. J.; Gell, C.; Ma, Z.; Graves, B.; Jackson, D.; Lee, K.; Juarez, R.; Koranteng, J.; Muntaka, S.; Mitchell, D. A.; da Silva, A. C.; Hussain, F.; Yilmaz, G.; Mastrotto, F.; Irie, Y.; Williams, P.; Williams, D. L.; Cámara, M.; Martinez-Pomares, L. Carbohydrates from Pseudomonas aeruginosa biofilms interact with immune C-type Lectins and interfere with their receptor function. *NPJ Biofilms Microbiomes* **2021**, *7* (1), 1−14.

(12) Chiffoleau, E. C-type lectin-like receptors as emerging orchestrators of sterile inflammation represent potential therapeutic targets. *Front. Immunol.* **2018**, *9*, 227.
(13) Geijtenbeek, T. B.; Torensma, R.; van Vliet, S. J.; van Duijnhoven, G. C.; Adema, G. J.; van Kooyk, Y.; Figdor, C. G. Identification of DC-SIGN, a novel dendritic cell−specific ICAM-3 receptor that supports primary immune responses. *Cell* **2000**, *100* (5), 575−585.
(14) Geijtenbeek, T. B. H.; Kwon, D. S.; Torensma, R.; van Vliet, S. J.; van Duijnhoven, G. C. F.; Middel, J.; Cornelissen, I. L. M. H. A.; Nottet, H. S. L. M.; KewalRamani, V. N.; Littman, D. R.; Figdor, C. G.; van Kooyk, Y. DC-SIGN, a dendritic cell−specific HIV-1-binding protein that enhances trans-infection of T cells. *Cell* **2000**, *100* (5), 587−597.
(15) Koning, N.; Kessen, S. F. M.; Van Der Voorn, J. P.; Appelmelk, B. J.; Jeurink, P. V.; Knippels, L. M. J.; Garssen, J.; Van Kooyk, Y. Human milk blocks DC-SIGN−pathogen interaction via MUC1. *Front. Immunol.* **2015**, *6*, 112.
(16) Rahimi, N. C-type Lectin CD209L/L-SIGN and CD209/DC-SIGN: Cell Adhesion Molecules Turned to Pathogen Recognition Receptors. *Biology (Basel)* **2021**, *10* (1), 1−15.
(17) van Kooyk, Y.; Geijtenbeek, T. B. DC-SIGN: escape mechanism for pathogens. *Nat. Rev. Immunol.* **2003**, *3* (9), 697−709.
(18) Garcia-Vallejo, J. J.; van Kooyk, Y. DC-SIGN: the strange case of Dr. *Jekyll and Mr. Hyde. Immunity* **2015**, *42* (6), 983−985.
(19) Wexler, H. M. Bacteroides: the good, the bad, and the nitty-gritty. *Clin. Microbiol. Rev.* **2007**, *20* (4), 593−621.
(20) Wang, C.; Xiao, Y.; Yu, L.; Tian, F.; Zhao, J.; Zhang, H.; Chen, W.; Zhai, Q. Protective effects of different Bacteroides vulgatus strains against lipopolysaccharide-induced acute intestinal injury, and their underlying functional genes. *J. Adv. Res.* **2022**, *36*, 27−37.
(21) Li, S.; Wang, C.; Zhang, C.; Luo, Y.; Cheng, Q.; Yu, L.; Sun, Z.; Chen, T. Evaluation of the Effects of Different *Bacteroides vulgatus* Strains against DSS-Induced Colitis. *J. Immunol. Res.* **2021**, *2021*, No. 9117805.
(22) Wexler, A. G.; Goodman, A. L. An insider's perspective: Bacteroides as a window into the microbiome. *Nat. Microbiol.* **2017**, *2* (5), 17026.
(23) Di Lorenzo, F.; Pither, M. D.; Martufi, M.; Scarinci, I.; Guzmán-Caldentey, J.; Łakomiec, E.; Jachymek, W.; Bruijns, S. C. M.; Santamaría, S. M.; Frick, J.-S.; van Kooyk, Y.; Chiodo, F.; Silipo, A.; Bernardini, M. L.; Molinaro, A. Pairing Bacteroides vulgatus LPS Structure with Its Immunomodulatory Effects on Human Cellular Models. *ACS Cent. Sci.* **2020**, *6* (9), 1602−1616.
(24) Zhu, Q.; Shen, Z.; Chiodo, F.; Nicolardi, S.; Molinaro, A.; Silipo, A.; Yu, B. Chemical synthesis of glycans up to a 128-mer relevant to the O -antigen of Bacteroides vulgatus. *Nat. Commun.* **2020**, *11* (1), 4142.
(25) Di Carluccio, C.; Forgione, M. C.; Martini, S.; Berti, F.; Molinaro, A.; Marchetti, R.; Silipo, A. Investigation of protein-ligand complexes by ligand-based NMR methods. *Carbohydr. Res.* **2021**, *503*, No. 108313.
(26) Feinberg, H.; Mitchell, D. A.; Drickamer, K.; Weis, W. I. Structural basis for selective recognition of oligosaccharides by DC-SIGN and DC-SIGNR. *Science* **2001**, *294* (5549), 2163−2166.
(27) Schrödinger, L., Schrödinger, LLC: New York, NY, 2017, *The PyMol. Molecular Graphics System*, Version 2017, 2.
(28) Feinberg, H.; Castelli, R.; Drickamer, K.; Seeberger, P. H.; Weis, W. I. Multiple modes of binding enhance the affinity of DC-SIGN for high mannose N-linked glycans found on viral glycoproteins. *J. Biol. Chem.* **2007**, *282* (6), 4202−4209.
(29) Cramer, J.; Lakkaichi, A.; Aliu, B.; Jakob, R. P.; Klein, S.; Cattaneo, I.; Jiang, X.; Rabbani, S.; Schwardt, O.; Zimmer, G.; Ciancaglini, M.; Abreu Mota, T.; Maier, T.; Ernst, B. Sweet Drugs for Bad Bugs: A Glycomimetic Strategy against the DC-SIGN-Mediated Dissemination of SARS-CoV-2. *J. Am. Chem. Soc.* **2021**, *143* (42), 17465−17478.
(30) Jayalakshmi, V.; Krishna, N. R. Complete Relaxation and Conformational Exchange Matrix (CORCEMA) Analysis of Intermolecular Saturation Transfer Effects in Reversibly Forming ligand−receptor Complexes. *J. Magn. Reson.* **2002**, *155* (1), 106−118.
(31) Guzzi, C.; Alfarano, P.; Sutkeviciute, I.; Sattin, S.; Ribeiro-Viana, R.; Fieschi, F.; Bernardi, A.; Weiser, J.; Rojo, J.; Angulo, J.; Nieto, P. M. Detection and quantitative analysis of two independent binding modes of a small ligand responsible for DC-SIGN clustering. *Org. Biomol. Chem.* **2016**, *14* (1), 335−44.
(32) Guo, Y.; Feinberg, H.; Conroy, E.; Mitchell, D. A.; Alvarez, R.; Blixt, O.; Taylor, M. E.; Weis, W. I.; Drickamer, K. Structural basis for distinct ligand-binding and targeting properties of the receptors DC-SIGN and DC-SIGNR. *Nat. Struct. Mol. Biol.* **2004**, *11* (7), 591−598.
(33) Li, Y.; Yang, Y.; Yu, B. An efficient glycosylation protocol with glycosyl ortho-alkynylbenzoates as donors under the catalysis of Ph3PAuOTf. *Tetrahedron Lett.* **2008**, *49* (22), 3604−3608.
(34) Porkolab, V.; Pifferi, C.; Sutkeviciute, I.; Ordanini, S.; Taouai, M.; Thépaut, M.; Vivès, C.; Benazza, M.; Bernardi, A.; Renaudet, O.; Fieschi, F. Development of C-type lectin-oriented surfaces for high avidity glycoconjugates: towards mimicking multivalent interactions on the cell surface. *Org. Biomol. Chem.* **2020**, *18* (25), 4763−4772.
(35) Sattin, S.; Daghetti, A.; Thépaut, M.; Berzi, A.; Sánchez-Navarro, M.; Tabarani, G.; Rojo, J.; Fieschi, F.; Clerici, M.; Bernardi, A. Inhibition of DC-SIGN-Mediated HIV Infection by a Linear Trimannoside Mimic in a Tetravalent Presentation. *ACS Chem. Biol.* **2010**, *5* (3), 301−312.
(36) Zhang, Y.; Wang, L.; Zhou, Q.; Li, Z.; Li, D.; Yin, C.; Wang, X.; Xiao, G. Modular Synthesis of a Tridecasaccharide Motif of Bacteroides vulgatus Lipopolysaccharides against Inflammatory Bowel Diseases through an Orthogonal One-Pot Glycosylation Strategy. *Angew. Chem., Int. Ed.* **2023**, *62* (22), No. e202301351.
(37) Case, D. A.; Ben-Shalom, I. Y.; Brozell, S. R.; Cerutti, D. S.; Cheatham, T. E.; Cruzeiro, V. W. D.; Darden, T. A.; Duke, R. E.; Ghoreishi, D.; Gilson, M. K.; Gohlke, H.; Goetz, A. W.; Greene, D.; Harris, R.; Homeyer, N.; Huang, Y.; Izadi, S.; Kovalenko, A.; Kurtzman, T.; Lee, T. S.; LeGrand, S.; Li, P.; Lin, C.; Liu, J.; Luchko, T.; Luo, R.; Mermelstein, D. J.; Merz, K. M.; Miao, Y.; Monard, G.; Nguyen, C.; Nguyen, H.; Omelyan, I.; Onufriev, A.; Pan, F.; Qi, R.; Roe, D. R.; Roitberg, A.; Sagui, C.; Schott-Verdugo, S.; Shen, J.; Simmerling, C. L.; Smith, J.; SalomonFerrer, R.; Swails, J.; Walker, R. C.; Wang, J.; Wei, H.; Wolf, R. M.; Wu, X.; Xiao, L.; York, M.; Kollman, P. A. *AMBER 2018*; University of California: San Francisco, 2018.
(38) Valverde, P.; Delgado, S.; Martínez, J. D.; Vendeville, J.-B.; Malassis, J.; Linclau, B.; Reichardt, N.-C.; Cañada, F. J.; Jimenez-Barbero, J.; Arda, A. Molecular insights into DC-SIGN binding to self-antigens: The interaction with the blood group A/B antigens. *ACS Chem. Biol.* **2019**, *14* (7), 1660−1671.
(39) Akira, S.; Uematsu, S.; Takeuchi, O. Pathogen recognition and innate immunity. *Cell* **2006**, *124* (4), 783−801.
(40) Mnich, M. E.; Van Dalen, R.; Van Sorge, N. M. C-type lectin receptors in host defense against bacterial pathogens. *Front. Cell. Infect. Microbiol.* **2020**, *10*, 309.
(41) Rabinovich, G. A.; Van Kooyk, Y.; Cobb, B. A. Glycobiology of immune responses. *Ann. N.Y. Acad. Sci.* **2012**, *1253* (1), 1−15.
(42) Molinaro, A.; Holst, O.; Di Lorenzo, F.; Callaghan, M.; Nurisso, A.; D'Errico, G.; Zamyatina, A.; Peri, F.; Berisio, R.; Jerala, R.; Jiménez-Barbero, J.; Silipo, A.; Martín-Santamaría, S. Chemistry of Lipid A: At the Heart of Innate Immunity. *Chem.—Eur. J.* **2015**, *21* (2), 500−519.
(43) Martínez-López, M.; Iborra, S.; Conde-Garrosa, R.; Mastrangelo, A.; Danne, C.; Mann, E. R.; Reid, D. M.; Gaboriau-Routhiau, V.; Chaparro, M.; Lorenzo, M. P.; Minnerup, L.; Saz-Leal, P.; Slack, E.; Kemp, B.; Gisbert, J. P.; Dzionek, A.; Robinson, M. J.; Rupérez, F. J.; Cerf-Bensussan, N.; Brown, G. D.; Bernardo, D.; LeibundGut-Landmann, S.; Sancho, D. Microbiota sensing by Mincle-Syk axis in dendritic cells regulates interleukin-17 and-22 production and promotes intestinal barrier integrity. *Immunity* **2019**, *50* (2), 446−461.

https://doi.org/10.1021/jacsau.3c00748
JACS Au 2024, 4, 697−712

(44) Garcia-Vallejo, J. J.; Van Kooyk, Y. *DC-sign. C-type lectin with prominent role in immune system*. SpringerReference: 2015; p 649−659.
(45) Michaelis, L.; Treß, M.; Löw, H.-C.; Klees, J.; Klameth, C.; Lange, A.; Grießhammer, A.; Schäfer, A.; Menz, S.; Steimle, A.; Schulze-Osthoff, K.; Frick, J.-S. Gut Commensal-Induced IκBζ Expression in Dendritic Cells Influences the Th17 Response. *Front. Immunol.* **2021**, *11*, No. 612336.
(46) van Liempt, E.; Bank, C. M.; Mehta, P.; Garcı, J. J.; Kawar, Z. S.; Geyer, R.; Alvarez, R. A.; Cummings, R. D.; van Kooyk, Y.; van Die, I. Specificity of DC-SIGN for mannose-and fucose-containing glycans. *FEBS Lett.* **2006**, *580* (26), 6123−6131.
(47) Bloem, K.; Garcia-Vallejo, J. J.; Vuist, I. M.; Cobb, B. A.; van Vliet, S. J.; van Kooyk, Y. Interaction of the Capsular Polysaccharide A from Bacteroides fragilis with DC-SIGN on Human Dendritic Cells is Necessary for Its Processing and Presentation to T Cells. *Front. Immunol.* **2013**, *4*, 103.
(48) Klena, J.; Zhang, P.; Schwartz, O.; Hull, S.; Chen, T. The core lipopolysaccharide of Escherichia coli is a ligand for the dendritic-cell-specific intercellular adhesion molecule nonintegrin CD209 receptor. *J. Bacteriol.* **2005**, *187* (5), 1710−1715.
(49) Zhang, P.; Schwartz, O.; Pantelic, M.; Li, G.; Knazze, Q.; Nobile, C.; Radovich, M.; He, J.; Hong, S. C.; Klena, J.; Chen, T. DC-SIGN (CD209) recognition of Neisseria gonorrhoeae is circumvented by lipooligosaccharide variation. *J. Leukocyte Biol.* **2006**, *79* (4), 731−738.
(50) Garcia-Vallejo, J. J.; van Kooyk, Y. The physiological role of DC-SIGN: a tale of mice and men. *Trends Immunol.* **2013**, *34* (10), 482−486.
(51) Zhang, P.; Snyder, S.; Feng, P.; Azadi, P.; Zhang, S.; Bulgheresi, S.; Sanderson, K. E.; He, J.; Klena, J.; Chen, T. Role of N-acetylglucosamine within core lipopolysaccharide of several species of gram-negative bacteria in targeting the DC-SIGN (CD209). *J. Immunol.* **2006**, *177* (6), 4002−4011.
(52) Nieto-Fabregat, F.; Marseglia, A.; Thépaut, M.; Kleman, J. P.; Abbas, M.; Le Roy, A.; Ebel, C.; Maalej, M.; Simorre, J. P.; Laguri, C.; Molinaro, A.; Silipo, A.; Fieschi, F.; Marchetti, R. Molecular Recognition of Escherichia Coli Core Lipooligosaccharide by DC-SIGN. *iScience* **2024**, *27*, No. 108792.
(53) Lee, R. T.; Hsu, T.-L.; Huang, S. K.; Hsieh, S.-L.; Wong, C.-H.; Lee, Y. C. Survey of immune-related, mannose/fucose-binding C-type lectin receptors reveals widely divergent sugar-binding specificities. *Glycobiology* **2011**, *21* (4), 512−520.
(54) Porkolab, V.; Lepšík, M.; Ordanini, S.; St John, A.; Le Roy, A.; Thépaut, M.; Paci, E.; Ebel, C.; Bernardi, A.; Fieschi, F. Powerful avidity with a limited valency for virus-attachment blockers on DC SIGN: Combining chelation and statistical rebinding with structural plasticity of the receptor. *ACS Cent. Sci.* **2023**, *9* (4), 709−718.
(55) Jarvis, C. M.; Zwick, D. B.; Grim, J. C.; Alam, M. M.; Prost, L. R.; Gardiner, J. C.; Park, S.; Zimdars, L. L.; Sherer, N. M.; Kiessling, L. L. Antigen structure affects cellular routing through DC-SIGN. *Proc. Natl. Acad. Sci. U.S.A.* **2019**, *116* (30), 14862−14867.
(56) Hoving, J. C.; Wilson, G. J.; Brown, G. D. Signalling C-type lectin receptors, microbial recognition and immunity. *Cell. Microbiol.* **2014**, *16* (2), 185−194.
(57) Woods Group *GLYCAM Web Complex Carbohydrate Research Center*; University of Georgia: Athens, GA, 2005.
(58) *Schrödinger Release 2022*−3; Maestro, Schrödinger, LLC: New York, 2021.
(59) Roe, D. R.; Cheatham, T. E., III PTRAJ and CPPTRAJ: software for processing and analysis of molecular dynamics trajectory data. *J. Chem. Theory Comput.* **2013**, *9* (7), 3084−3095.
(60) Humphrey, W.; Dalke, A.; Schulten, K. VMD - Visual Molecular Dynamics. *J. Mol. Graphics* **1996**, *14*, 33−38.
(61) Pettersen, E. F.; Goddard, T. D.; Huang, C. C.; Couch, G. S.; Greenblatt, D. M.; Meng, E. C.; Ferrin, T. E. UCSF Chimera–a visualization system for exploratory research and analysis. *J. Comput. Chem.* **2004**, *25* (13), 1605−12.
(62) Tabarani, G.; Thépaut, M.; Stroebel, D.; Ebel, C.; Vivès, C.; Vachette, P.; Durand, D.; Fieschi, F. DC-SIGN Neck Domain Is a pH-sensor Controlling Oligomerization: Saxs and Hydrodynamic Studies of Extracellular Domain. *J. Biol. Chem.* **2009**, *284* (32), 21229−21240.
(63) Halary, F.; Amara, A.; Lortat-Jacob, H.; Messerle, M.; Delaunay, T.; Houlès, C.; Fieschi, F.; Arenzana-Seisdedos, F.; Moreau, J. F.; Déchanet-Merville, J. Human cytomegalovirus binding to DC-SIGN is required for dendritic cell infection and target cell trans-infection. *Immunity* **2002**, *17* (5), 653−64.
(64) Andreini, M.; Doknic, D.; Sutkeviciute, I.; Reina, J. J.; Duan, J.; Chabrol, E.; Thepaut, M.; Moroni, E.; Doro, F.; Belvisi, L.; Weiser, J.; Rojo, J.; Fieschi, F.; Bernardi, A. Second generation of fucose-based DC-SIGN ligands: affinity improvement and specificity versus Langerin. *Org. Biomol. Chem.* **2011**, *9* (16), 5778−5786.

https://doi.org/10.1021/jacsau.3c00748
JACS Au 2024, 4, 697−712